Enhanced hemato-endothelial specification during human embryonic differentiation through developmental cooperation between *AF4-MLL* and *MLL-AF4* fusions

Clara Bueno[1,6]*, Fernando J Calero-Nieto[2], Xiaonan Wang[2], Rafael Valdés-Mas[3], Francisco Gutiérrez-Agüera[1], Heleia Roca-Ho[1], Veronica Ayllon[4], Pedro J Real[4], David Arambilet[5], Lluis Espinosa[5,6], Raul Torres-Ruiz[1], Antonio Agraz-Doblas[1,7], Ignacio Varela[7], Jasper de Boer[8], Anna Bigas[5,6], Bertie Gottgens[2], Rolf Marschalek[9], Pablo Menendez[1,6,10]*

[1]Josep Carreras Leukemia Research Institute and Department of Biomedicine, School of Medicine. University of Barcelona. Barcelona. Spain. [2]Department of Hematology, Cambridge Institute for Medical Research and Wellcome Trust-Medical Research Council Cambridge Stem Cell Institute, University of Cambridge, United Kingdom. [3]Dreamgenics S.L. Oviedo. Spain. [4]GENyO, Centre for Genomics and Oncological Research, Pfizer/University of Granada/Andalusian Regional Government and University of Granada, Department of Biochemistry and Molecular Biology, Granada, Spain. [5]Programa de Cáncer. Instituto Hospital del Mar de Investigaciones Médicas. Barcelona. Spain. [6]Centro de Investigación Biomédica en Red de Cáncer (CIBER-ONC), ISCIII, Barcelona, Spain. [7]Instituto de Biomedicina y Biotecnología de Cantabria (CSIC-UC-Sodercan), Departamento de Biología Molecular, Universidad de Cantabria, Santander, Spain. [8]Cancer Section, UCL Great Ormond Street Institute of Child Health, London, United Kingdom. [9]Institute of Pharmaceutical Biology, Goethe-University. Frankfurt. Germany. [10]Instituciò Catalana de Recerca i Estudis Avançats (ICREA). Barcelona. Spain.

Running Title: AF4-MLL in human embryonic hematopoietic development

Key words: AF4-MLL, MLL-AF4, HOX cluster, human ESC, hemato-endothelial specification.

*Correspondence should be addressed to:

Clara Bueno PhD & Pablo Menendez PhD
Josep Carreras Leukemia Research Institute
School of Medicine. University of Barcelona.
Casanova 143, 08036. Barcelona. Spain.
cbueno@carrerasresearch.org ; pmenendez@carrerasresearch.org

ABSTRACT

The t(4;11)(q21;q23) translocation is associated with high-risk infant pro-B-cell acute lymphoblastic leukemia and arises prenatally during embryonic/fetal hematopoiesis. The developmental/pathogenic contribution of the t(4;11)-resulting *MLL-AF4* (MA4) and *AF4-MLL* (A4M) fusions remains unclear; MA4 is always expressed in t(4;11)+ B-cell acute lymphoblastic leukemia patients, but the reciprocal fusion A4M is expressed in only half of the patients. Because prenatal leukemogenesis manifests as impaired early hematopoietic differentiation, we took advantage of well-established human embryonic stem cell-based hematopoietic differentiation models to study whether the A4M fusion cooperates with MA4 during early human hematopoietic development. Co-expression of A4M and MA4 strongly promoted the emergence of hemato-endothelial precursors, both endothelial- and hemogenic-primed. Double fusion-expressing hemato-endothelial precursors specified into significantly higher numbers of both hematopoietic and endothelial-committed cells, irrespective of the differentiation protocol used and without hijacking survival/proliferation. Functional analysis of differentially expressed genes and differentially enriched H3K79me3 genomic regions by RNA-seq and H3K79me3 ChIP-seq, respectively, confirmed a hematopoietic/endothelial cell differentiation signature in double fusion-expressing hemato-endothelial precursors. Importantly, ChIP-seq analysis revealed a significant enrichment of H3K79 methylated regions specifically associated with *HOX-A* cluster genes in double fusion-expressing differentiating hematopoietic cells. Overall, these results establish a functional and molecular cooperation between MA4 and A4M fusions during human hematopoietic development.

INTRODUCTION

The mixed-lineage leukemia (*MLL*) gene encodes for an H3K4 histone methyltransferase important in hematopoietic development[1]. The human *MLL* gene is frequently rearranged in acute leukemia and typically confers a dismal outcome[2, 3]. Of particular interest is the translocation t(4;11)(q21;q23), which encodes the fusion proteins *MLL-AF4* (*MA4*) and *AF4-MLL* (*A4M*), and is associated with infant B-cell acute lymphoblastic leukemia (B-ALL). This t(4;11)+ infant leukemia is characterized by a very brief latency, raising the question of how it evolves so quickly[4]. Moreover, the exceptionally high concordance rate of t(4;11)+ B-ALL in monozygotic twin infants[5, 6] suggests that all the necessary (epi)genetic events required for leukemogenesis are accomplished prenatally, during embryonic/fetal hematopoietic development[7]. However, our understanding of t(4;11)-mediated developmental effects is limited, at least in part, due to the variety of phenotypes and long latency observed in currently available t(4;11) mouse models[2, 8-17]. These different phenotypes likely result from targeting a cell in the wrong developmental stage, or not addressing the impact of secondary hits, leaving open questions about the developmental impact of the t(4;11) translocation during early human development.

The functional and molecular contribution of the reciprocal fusion genes resulting from the derivative translocated chromosomes remains obscure in cancer. The MA4 fusion is always expressed in t(4;11)+B-ALL patients, whereas the reciprocal fusion A4M is expressed in only half of the patients[18-20]. Importantly, t(4;11)+ cell lines display addiction to MA4 but not to A4M[21, 22], and although A4M was not sufficient to initiate leukemia in cord blood-derived CD34+ cells[23], it was nevertheless capable of initiating B-ALL in mice without the requirement of MA4, indicating that it contributes to t(4;11)-driven leukemogenesis[11, 24, 25]. Strikingly, a very recent clinical study have unraveled an independent prognostic value for MA4 expression in t(4;11)+ infant B-ALL, thus adding a new piece to the puzzle[19]. Thus, the developmental/pathogenic contribution of the t(4;11)-resulting reciprocal fusion A4M remains enigmatic.

Human embryonic stem cells (hESCs) represent a powerful tool for modeling different developmental aspects of human disease that cannot otherwise be addressed by patient sample analyses or mouse models[7, 26, 27]. Because prenatal leukemogenesis manifests as impaired early hematopoietic differentiation, modeling hematopoietic differentiation in hESCs may represent a promising *in vitro* approach to study the onset of hematopoiesis and the mechanisms underlying early human hematopoietic development[7]. During hESC differentiation, a primitive population of CD45- hemato-endothelial precursors (HEPs) arises and further differentiates into CD45+ hematopoietic and mature endothelial cells[28-30]. Beyond their pathogenic role in acute leukemias, the *MLL* gene has also been implicated in endothelial cell maturation[31], and endothelial dysfunction was recently linked to disease outcomes in childhood leukemias[32]. We previously reported that MA4 favors the emergence of endothelial-primed HEPs but not hemogenic HEPs from hESCs[10]. Here, we took advantage of well-established hESC-based differentiation systems to study whether the A4M fusion cooperates with MA4 during early human hematopoietic and endothelial development. We report a functional and molecular cooperation between MA4 and A4M fusions, which results in an enhanced hemato-endothelial output during human embryonic development.

METHODS

Vector construction and lentiviral transduction

The cDNAs for MA4 and A4M were subcloned into the pRRL-EF1α-PGK-NEO vector[11, 16]. Both fusions have been described previously (FigS1A)[11, 23]. We used the following lentivectors containing either neomycin or dTo for cell selection: pRRL-EF1α-PGK-NEO (empty vector;EV), pRRL-EF1α-MA4-PGK-NEO (MA4) and pRRL-EF1α-A4M-PGK-dTo (A4M). VSV-G-pseudotyped lentiviral particles were generated in 293T cells using standard transfection protocols and concentrated by ultracentrifugation[33]. hESCs were infected overnight with concentrated EV or MA4 lentivirus plus 8 μg/ml polybrene. Viral supernatants were washed away the next day, and EV- and MA4-transduced hESCs were then selected with G418 (50-100μg/ml) for three weeks. For dual transduction of MA4 and A4M fusions, G418-resistant MA4-expressing hESCs were infected with A4M-expressing viruses. EV/G418-selected hESCs were also transduced with A4M alone. Transgene expression was confirmed for all the genotypes (Fig1).

Human ESC culture and characterization of transgenic human ESC lines

hESCs (AND1 line) were maintained undifferentiated on a layer of irradiated-hMSCs (iMSC) in complete KO-DMEM medium containing 20% knockout serum replacement and 8 ng/mL basic fibroblast growth factor (bFGF)[34, 35]. The medium was changed daily, and cells were passaged weekly by dissociation with 1:1 collagenase IV:Dispase. Cultures were visualized daily by phase contrast microscopy. Approval for hESC work was obtained from the Spanish National Embryo Ethical Committee. Pluripotency of transgenic hESCs was characterized by flow cytometry using antibodies against SSEA-3, SSEA-4 TRA-1-60 and TRA-1-81 (BD Biosciences)[36]. Expression of the pluripotency-associated transcription factors *OCT4*, *NANOG*, *SOX2*, *CRIPTO*, and *DNMT3B* as well as transgene expression (*MA4* and *A4M*) were analyzed by qRT-PCR. TableS1 shows the primers and PCR conditions used[23, 37, 38].

Hematopoietic differentiation from human ESCs by embryoid body formation.

Undifferentiated hESCs were treated with collagenase IV:Dispase for 1 hr at 37ºC. For embryoid body (EB) formation, cells were transferred to low-attachment plates and incubated overnight in differentiation medium (DM; KO-DMEM supplemented with 20% FBS, 1% nonessential amino acids, 1 mmol/L L-glutamine, and 0.1 mmol/L β-mercaptoethanol). The medium was changed next day to the same DM supplemented with the following hematopoietic cytokines: 300 ng/mL stem cell factor (SCF), 300 ng/mL Flt3L, 10 ng/mL interleukin (IL)-3, 10 ng/mL IL-6, 50 ng/mL granulocyte-colony stimulating factor (G-CSF) and 25 ng/mL bone morphogenetic protein 4 (BMP-4) (all from R&D)[9, 29, 39-41]. EBs were dissociated at different time points during development using collagenase B and enzyme-free Cell Dissociation Buffer (Invitrogen). Dissociated cells were stained with anti-CD34-PE, anti-CD31-FITC, anti-CD45-APC or anti-CD34-PE-Cy7, CD31-BV510, anti-Glycophorin A, anti-CD43-FITC, anti-CD45-APC antibodies (all from BD Biosciences) and 7-actinomycin D, and analyzed using a FACS Canto flow cytometer[9, 29, 39-41]. Colony-forming unit (CFU) assays were performed at day 10 and 15 of EB differentiation by plating $60x10^4$ EB cells onto serum-free methylcellulose H4435 (Stem Cell Technologies). Colonies were scored after 12 days[9, 29, 42-44].

Cell cycle and apoptosis analysis

For cell cycle analysis of hESC-derived HEPs and $CD45^+$ cells, day 15 EBs were dissociated and harvested cells were fixed overnight in 70% ice-cold ethanol. Cells were then washed in PBS and incubated with anti-CD31-FITC, anti-CD34-PE-Cy7 and anti-CD45-APC antibodies for 15 min. Cells were then suspended in propidium iodide-containing buffer and acquired-analysed on a FACS Canto-II using Modfit LT4.0 software, discriminating between quiescent cells (G0/G1), cycling cells (S-phase) and G2/M cells[45, 46]. Apoptosis was assessed with the Annexin-V apoptosis detection kit (BD Biosciences)[16].

Human ESC-OP9 co-cultures

hESC-OP9 co-cultures were performed as described[47, 48]. OP9 stroma was prepared by plating OP9 cells in gelatin-coated dishes, and allowing them to overgrow as a monolayer. hESCs were prepared as a suspension of small aggregates using collagenase IV:Dispase. One-tenth of this suspension was plated on top of the 8-day overgrown OP9 stroma. Media was replaced on the next day and one-half volume media changes were performed every other day thereafter. Hematopoietic differentiation was assessed by flow cytometry at day 9 of co-culture. Accordingly, hESC-OP9 co-cultures were treated with collagenase IV/TrypLE and cells were dissociated and filtered through a 70-μm strainer. Cell suspensions were stained with anti-mouse CD29-FITC and anti-human CD34-PE and CD45-APC antibodies. The proportion of HEPs ($CD34^+CD31^+CD45^-$), and total blood cells ($CD45^+$) was analyzed within the $CD29^-$ human ESC-derived cell population. Hemogenic and endothelial HEPs were distinguished based on CD34 and CD43 expression[40].

Culture of FACS-isolated HEPs in MS5 stroma or liquid culture

Day 9 human hESC-OP9 co-cultures were dissociated as above and both CD45+ cells and HEPs were analyzed. FACS-purified HEPs ($CD29^-CD34^+CD31^+CD45^-$) were plated onto MS5 stroma or in liquid culture for 30 or 16 days, respectively, in DM with hematopoietic cytokines (50 ng/mL SCF, 50 ng/mL Flt3L, 10 ng/mL IL-3,20 ng/mL IL-7). The medium was changed every 7 days, and the emergence of CD45+ hematopoietic cells was analyzed by FACS.

Endothelial differentiation of HEPs

HEPS (2×10^4) from day 9 human hESC-OP9 co-cultures were seeded onto 0.1% gelatin-coated plates in complete EGM-2 medium with microvasculature supplements (Lonza) for 7 days. Cells were then fixed, permeabilized and stained with rabbit anti-human VE-cadherin (Cayman), mouse anti-human eNOS (BD Biosciences), and mouse anti-human vWF (DAKO) followed by Alexa488-conjugated anti-rabbit or Cy3-

conjugated anti-mouse (Jakson Immunoresearch) antibodies. Nuclei were counterstained with DAPI. Images were obtained using an inverted fluorescence microscope. Day 7 differentiating cells were trypsinized and cell suspensions were stained with anti-human CD31-FITC and CD144-PerCP-Cy5.5 antibodies.

Mouse transplantation and analysis of hematopoietic-endothelial engraftment

NOD/LtSz-scid IL-2Rγ$^{-/-}$ (NSG) mice were housed under sterile conditions. The Animal Care Committee approved all mouse protocols. Briefly, cord bood-derived CD34^{+} HSPCs (3×10^4 cells) or cells from day 15 EBs (5×10^5 cells) were intra-bone marrow (BM)-transplanted as described[49]. Animal health was monitored throughout the entire experiment. Mice were killed 10 weeks after transplantation and cell suspensions were analyzed by FACS for human chimerism using anti-HLA-ABC-FITC, anti-CD31-PE, CD144-PerCP-Cy5.5, and anti-CD45-APC antibodies.

Statistical analysis

All data are expressed as mean±SEM. Statistical comparisons were performed using the GraphPad Prism software with the nonparametric Mann-Whitney test, two-tailed P-value (95% confidence interval). Statistical significance was defined as a p-value<0.05.

Online methods show detailed information about RNA- and Chromatin Immunoprecipitation sequencing and analysis.

RESULTS

Co-expression of A4M and MA4 does not hijack pluripotency

We showed very recently that only 45% of t(4;11)+ B-ALL patients express the reciprocal fusion A4M, whereas MA4 is consistently expressed in all t(4;11)+ B-ALL patients (Fig1A)[18-20]. Here, we generated transgenic hESC lines expressing "MA4 alone", "A4M alone" or MA4+A4M (double fusion, Fig1B, S1B). EV (control)- and MA4-hESCs were established by G418 selection[9]. G418-resistant EV- or MA4-expressing hESCs were then transduced with A4M/dTo-expressing lentiviruses and >90% transduction efficiency was achieved. Transgenic hESC lines were maintained for >50 passages and retained human ESC-like morphology (Fig1B, left), transgene expression (Fig1B, right), and expression of pluripotency-associated transcription factors (Fig1C) and surface markers (Fig1D). All hESC genotypes formed teratomas in NSG mice (data not shown)[9, 50]. Thus, (co-)expression of A4M and/or MA4 is compatible with hESC pluripotency.

A4M and MA4 co-operate to promote HEPs emergence and enhance blood production

Hematopoietic differentiation was assessed using two distinct and well-established differentiation systems: EB formation[43, 47] (Fig2) and OP9 co-culture[47, 48] (Fig3). During differentiation, a population of primitive HEPs arises, which is responsible for further hematopoietic and endothelial commitment[10, 30] (Fig2A,3A). We investigated whether co-expression of A4M and MA4 impacts hESC-derived hematopoiesis by analyzing the emergence of HEPs during EB development in hESCs individually expressing the single fusions or the double fusion. We observed a pronounced (~5-10-fold; $p<0.05$) increase in HEPs at day 7 and 10 of development in EBs expressing the double A4M and MA4 fusion over single fusions (Fig2B, upper-left panel). We next assessed whether co-expression of A4M and MA4 influences subsequent hematopoietic commitment of HEPs. The kinetics of emergence and output of both total $CD45^+$ hematopoietic cells and $CD45^+CD34^+$ hematopoietic progenitors was faster (EB day 10) from double fusion-expressing hESCs than from equivalent single fusion-expressing cells, achieving a 2-3-fold higher hematopoietic output by day 15 of EB development

(Fig2B). Furthermore, double fusion-expressing HEPs massively accelerated (EB day10) the emergence of clonogenic hematopoietic progenitors as compared to single fusion-expressing HEPs (Fig2B, bottom-right panel). According to our previous work, if the kinetics of hEB differentiation are extended allowing for a continuum HEP-to-blood transition, MA4-expressing hEBs display an enhanced HEP production coupled to an impaired blood output (EB day 20, Fig S2A) and clonogenic potential (EB day 15, Fig 2B). We confirmed stable expression of ectopic MA4 and A4M upon EB differentiation, supporting the link between genotype and phenotype (Fig2C).

We also investigated hematopoietic differentiation using the OP9 differentiation system (Fig3A,B), and by plating FACS-sorted HEPs in either hematopoietic liquid culture (Fig3C) or onto MS5 feeders (Fig3D). After 10 days on OP9 stroma, double fusion-expressing hESCs yielded a 10-fold higher number of CD45+ hematopoietic cells than did single fusion-expressing hESCs (Fig3B). Moreover, when HEPs were FACS-sorted from day 9 OP9 co-cultures and allowed to differentiate into CD45+ blood cells, the yield of CD45+ cells was up to 60-fold higher in double fusion-expressing HEPs than in single fusion-expressing HEPs. (Fig3C,D). Encouraged by these results, we next investigated whether ectopic expression of both A4M and MA4 confers *in vivo* engraftment capacity to hESC-derived hematopoietic derivatives. To do this, we transplanted 5×10^5 hESC hematopoietic derivatives from each genotype into myeloablated NSG mice[4, 43, 47], finding that, despite regulating hematopoietic development *in vitro*, double fusion-expression did not confer *in vivo* engraftment to hESC hematopoietic derivatives (Fig2D).

The increased hematopoietic output of double fusion-expressing hESCs might be the consequence of transgene-mediated proliferation/survival of the emerging HEPs or CD45+ cells. To address this, we analyzed cell cycle distribution (FigS2B) and apoptosis (FigS2C) within both HEPs and the CD45+ cell population. No differences in the proportion of either cycling HEPs or CD45+ cells were detected between

genotypes (25–36% for HEPs and 35–41% for CD45+ cells; FigS2B). Apoptotic levels were similarly low between the different genotypes of HEPs (6–8%) and CD45+ cells (5–7%) (FigS2C). Collectively, these results show that A4M cooperates with MA4 to induce HEP specification and blood commitment, without hijacking proliferation or survival of HEPs.

A4M and MA4 co-operate to enhance endothelial cell fate from HEPs

We next addressed the developmental impact of A4M in endothelial maturation from HEPs[10, 47]. We hypothesized that co-expression of A4M and MA4 in HEPs may (i) concomitantly promote subsequent endothelial and hematopoietic commitment or (ii) skew the hemato-endothelial commitment in favor of hematopoiesis. To test this, we analyzed the ability of HEPs to differentiate into mature endothelial cells. OP9-hESC co-cultures were dissociated on day 9 of development and HEPs were FACS-sorted and cultured for a week in endothelial-promoting conditions (Fig4A). The expression of the mature endothelial markers VE-cadherin (CD144), vWF, eNOS and CD31 was then analyzed. Irrespective of the genotype, HEPs cultured in endothelial conditions attached, became spindle-shaped, and formed VE-Cad+ endothelial-like structures co-expressing eNOS, vWF and CD31 (Fig4B,C, top panel). However, double fusion-expressing HEPs were more prone to differentiate into mature endothelial cells than single fusion-expressing HEPs. Accordingly, they yielded a 20-fold higher number of VE-Cad+ endothelial-like structures (Fig4C, top panel) and CD144+CD31+ endothelial cells (Fig4C, bottom panel). Interestingly, endothelial cells ($HLA.ABC^+CD31^+CD34^+CD144^+CD45^-CD43^-$) were found in the BM of mice transplanted with double fusion-expressing hESC blood derivatives at levels ~4-fold higher than in mice transplanted with single fusion-expressing cells (Fig4D).

Within $CD34^+CD31^+CD45^-$ HEPs, two subpopulations of phenotypically and functionally distinct HEPs can be distinguished based on the expression of CD34 and CD43: hemogenic HEPs ($CD34^{low/+}CD43^+CD45^-$) and

endothelial HEPs ($CD34^{++}CD43^{-}CD45^{-}$) (Fig5A)[40, 48, 51]. We thus analyzed the contribution of both HEP populations to the superior hematopoietic and endothelial differentiation observed in double fusion-expressing HEPs. Co-expression of A4M and MA4, but not single fusions, robustly enhanced the emergence of both endothelial and hemogenic HEPs (Fig5B,C). The identity of hemogenic and endothelial HEPs was confirmed by the specific expression of early hematopoietic and endothelial master genes (Fig5D). Thus, A4M cooperates with MA4 to promote hematopoietic and endothelial cell fate.

Genome-wide transcriptomic and H3K79 methylation profiles support the developmental cooperation between A4M and MA4

To identify patterns of gene expression that might molecularly explain the functional co-operation between A4M and MA4 in hematopoietic specification, we performed RNA-seq analysis on FACS-purified EV-, MA4, A4M- and double fusion-expressing HEPs from day 15 hEBs. Fig6A shows a heatmap representation of the hierarchical clustering of the 335 genes differentially expressed between the four genotypes (TableS2). There is a clear transcriptomic transition towards a hematopoietic/endothelial gene signature from EV-HEPs to double-fusion-expressing HEPs. Single fusion-expressing HEPs clustered interspersed between EV and double-fusion HEPs. The biological functions affected by genes differentially expressed in MA4-, A4M- and double fusion-expressing HEPs relative to EV were classified by IPA software[47, 52] and among the top significant enriched functional categories were “hematological system development and function”, “cancer” and “hematological disease” (Fig6B). Statistical (-log(p-value)) power shows distant effects of MA4 and A4M; however, co-expression of both fusions seems to establish a molecular balance/developmental cooperation in promoting blood-endothelial specification from hPSCs. Strikingly, biofunctions specifically associated to hematological lymphoid malignancies (not with non-hematological cancer) were predicted to be activated (positive z-score) exclusively in double fusion-expressing HEPs, further suggesting a molecular cooperation between MA4 and A4M in development and infant leukemia. (Fig6C).

The C-terminal-partners of MLL fusions normally interact with the histone methyltransferase DOT1L, which is the sole histone methyltransferase catalyzing histone 3 lysine 79 (H3K79) methylation, a chromatin modification widely associated with the dysregulated expression of *HOX-A* cluster genes in MLL leukemias [13, 53]. We thus performed genome-wide ChIP-seq analysis of the H3K79 trimethylation (H3K79me3) profiles in control, MA4-, A4M- and double fusion-expressing hESC-derived blood derivatives (Fig7,S3A, TableS3). In line with the RNA-seq data, functional analysis of the differential H3K79me3 peaks specific for double fusion-expressing cells revealed significant GO functional categories associated with "definitive hematopoiesis", "myeloid and erythroid differentiation/homeostasis" and "endothelial cell development" (Fig7A,S3B). This further supports the developmental co-operation between A4M and MA4 in promoting hemato-endothelial specification.

Finally, we analysed the H3K79me3 profiles at genomic loci of the classical MLL target genes reported by Guenther *et al*[54]. Non-*HOX-A* classical MLL targets such as *RUNX1*, *LMO2*, *ADMA10, and KDM6A* showed a slight although non-significant, enrichment of H3K79me3 in MA4-expressing hESCs, validating our ChIP-seq approach (Fig7B). However, enrichment of H3K79me3 in *HOX-A* cluster genes was observed exclusively in A4M-expressing cells although it was statistically significant only in double fusion-expressing differentiating hESCs (FDR<0.1) (Fig7C). As such, *HOX-A* genes were up-regulated in double-fusion-expressing hematopoietic clonogenic progenitors (FigS3C). No differential enrichment of the repressive H3K4me2/3 mark was observed in either *HOX-A* or non-*HOX* genes in double fusion-expressing cells (FigS4). Collectively, these data suggest that the deregulated expression of *HOX-A* genes in MLL leukemias may be imposed by the reciprocal A4M fusion through a H3K79 methyltransferase activity. In support of this, a recent RNA-seq study performed in 42 infants with t(4;11)+ B-ALL enrolled in the Interfant treatment protocol, reveal that 45% of t(4;11)+ patients express the A4M fusion, and that *HOX-A* cluster genes are

exclusively expressed in this *AF4-MLL*-expressing subgroup of t(4;11)+ patients, who in fact display a significant more favorable clinical outcome[19].

DISCUSSION

From an etiological and pathogenesis standpoint, infant cancer is distinct to adult cancer and should be studied as a developmental disease[4, 7, 16]. A biologically and clinically intriguing infant cancer is the t(4;11)+ B-ALL, which is associated with a dismal outcome[4, 21, 23]. Evidence in support of its prenatal origin comes from studies in monozygotic twins and archived blood spots, providing compelling evidence of a single prenatal cell as the origin for t(4;11)[5], and also from recent genome-wide studies demonstrating that this infant leukemia has one of the lowest frequencies of somatic mutations of any sequenced cancer[55]. The stable genome of these patients suggests that in infant developmental cancer, one "big-hit" might be sufficient for overt disease, supporting a key contribution of the prenatal cell-of-origin during a critical developmental window of stem cell vulnerability in leukemogenesis. However, despite its aggressiveness and short latency, our current understanding about its etiology, pathogenesis and cellular origin is still limited[2, 4, 14, 16, 52]. Importantly, a recently developed xenograft model which represents the most *bona fide* model for t(4;11)+ B-ALL so far, has revealed the instructive role of MLL-Af4 in cord blood-derived CD34+ cells[14].

Studies using primary cells from t(4;11)+ B-ALL patients are incapable of addressing the developmental genesis of the hematopoietic system. Recent data suggest that fetal liver lymphoid-primed multipotent progenitor may provide the developmental prerequisites for the initiation of t(4;11)+/MLL-AF4 infant leukemia[56]. Because leukemogenesis manifests as a blockage or altered cell differentiation, the hematopoietic differentiation of hESCs may represent a promising *in vitro* model to study the onset of hematopoiesis and the earliest events leading to the specification of the hematopoietic cells[36]. Previous studies have addressed the oncogenic role of leukemic fusion genes in hESC-derived hematopoiesis[57,58, 59].

We previously explored the developmental impact of the pre-natal fusion MA4 in hESC hemato-endothelial development[10], and found that MA4 expression promotes the emergence of endothelial-primed HEPs and further endothelial commitment, but hijacks the specification of hemogenic-primed HEPs, impairing hematopoietic output[10].

The functional and molecular contribution of the reciprocal fusion genes resulting from the derivative translocated chromosomes remains obscure in cancer[18, 60]. The MA4 fusion is always expressed in t(4;11)+B-ALL patients, whereas the reciprocal fusion A4M is expressed in only 45-50% of the patients[18, 60,19, 20]. Here, we took advantage of well-established hESC-based differentiation systems to study whether the A4M fusion cooperates with MA4 during early human hematopoietic and endothelial development. Co-expression of A4M and MA4 strongly promoted the emergence of HEPs, both endothelial-primed and hemogenic-primed. Moreover, the double fusion-expressing HEPs specified into significantly higher numbers of both hematopoietic and endothelial cells, irrespective of the *in vitro* differentiation protocol used and without affecting survival or proliferation, indicating a functional (developmental) co-operation between MA4 and A4M fusions during human hematopoietic development. This notion was confirmed by genome-wide transcriptomic analysis of differentiating HEPs. These developmental biology studies support previous evidence suggesting that A4M contributes to the pathobiology of t(4;11)+ B-ALL. Accordingly, Bursen[11] reported that A4M-transduced murine hematopoietic stem cells (HSCs) developed pro-B-ALL, whereas co-transduction with MA4 and A4M resulted in mixed lineage leukemia. Moreover, studies from Milne's laboratory demonstrated that RUNX1 is directly activated by MA4 and the RUNX1 protein interacts with the A4M protein, suggesting a mechanism of co-operation between the two fusion genes at the molecular level[25].

In the embryo, definitive hematopoiesis cannot occur in the absence of endothelial cell development. Definitive HSCs in both mouse and human emerge from the hemogenic endothelium by a process known as

endothelial-to-hematopoietic transition[61]. Hematopoietic differentiation of hESCs occurs through the generation of HEPs, from which then originate both endothelial and hematopoietic cells. Here, co-expression of A4M and MA4 in HEPs concomitantly promoted endothelial and hematopoietic commitment rather than skewing the hemato-endothelial commitment in favor of one lineage over the other. This finding is important because beyond their pathogenic role in acute leukemias, the *MLL* gene is implicated in endothelial cell maturation, and endothelial dysfunction was recently linked to disease outcome in childhood leukemias[31, 32]. Furthermore, other leukemia fusion oncogenes as well as lymphoma-specific genetic aberrations have been found in endothelial cells from chronic myeloid leukemia and B-cell lymphoma patients[10, 43, 44], suggesting that endothelial cells may be part of the neoplastic clone. Also, BM-derived mesenchymal stem cells (BM-MSCs) from infant t(4;11)+ B-cell ALL were recently found to harbor and express the t(4;11) translocation[33]. The existence of a common embryonic precursor for MSCs and endothelial cells has been recently demonstrated by hESC-directed differentiation[10, 45]. The finding of such a common embryonic precursor, and the presence of t(4;11) in both leukemic blasts and BM-MSCs of infant patients, suggests that the t(4;11) translocation arises and has a developmental impact on early pre-hematopoietic precursors. As a technical caveat, it is important to emphasize that MA4 and A4M were sequentially transduced to allow for antibiotic selection and homogeneously-transduced hESC cultures. However, in double-fusion-expressing differentiating blood cells, MA4 was never individually expressed in the absence of A4M. When hematopoietic differentiation of hESCs was induced by EB formation both fusions were readily co-expressed, ruling out a biased functional phenotype driven by the sequential expression of each transgene in distinct developmental windows.

Mechanistically, a putative function of A4M is to activate chromatin, rendering a chromatin landscape similar to that during stem cell development. It is currently unknown how A4M is able to reprogram chromatin, but it

does contain the SET domain disrupted from its "specification domain", the N-terminal portion of MLL, which binds to MEN1 and LEDGF, shaping the gene targeting module of the MLL gene. When A4M is expressed, the N-terminal portion is substituted by the AF4 N-terminus, which is the crucial domain (AF4N) that binds to and strongly activates RNA polymerase II (RNAP II) for transcriptional elongation. Overexpression of either AF4, AF4N or the fusion protein A4M induces robust RNAP II-dependent gene transcription by overwriting the elongation control process in a dominant fashion[62-64]. Since gene transcription *per se* and in particular “sterile” transcription is a powerful mechanism for chromatin activation, A4M could potentiate MA4 to skew normal and leukemic hematopoietic cell fate decisions. This also explains why MA4 has a more prominent role in the disease than the reciprocal A4M. If A4M functioned to initiate this process only by itself, then it would become obsolete after fulfilling the "chromatin opening job". However, transcription factors like MA4, RUNX1 or others then establish the transcriptional program leading to leukemogenesis. This is reflected in the enhanced hematopoietic potential of double fusion-expressing hESCs and the enriched H3K79me3 activation mark in *HOX-A* cluster genes exclusively when MA4 and A4M are co-expressed. Thus, A4M prepares other transcription factors to become oncoproteins.

Molecularly, C-terminal-partners of MLL fusions (AF4, AF9, ENL) interact with DOT1L, which is the sole histone methyltransferase catalyzing H3K79 methylation, a chromatin modification widely associated with the dysregulated expression of *HOX-A* gene cluster in MLL-rearranged leukemias[13, 53]. Here, ChIP-seq analysis of differentially enriched H3K79me3 genomic regions confirmed a hematopoietic/endothelial cell differentiation signature in double fusion-expressing HEPs, and revealed a significant enrichment of H3K79 methylated regions specifically associated with *HOX-A* cluster MLL target genes (but not to non-*HOX-A* MLL targets) in double fusion-expressing differentiating hematopoietic cells. This is in line with the recently found significant positive correlation between the upregulation of the *HOX-A* gene cluster and the expression of A4M in primary t(4;11)+ infant B-cell ALL samples, and with previous studies identifying that approximately

one-half of t(4;11)+ patients do not have an activated *HOX-A* signature[20, 65, 66]. This may explain why MA4 failed recently to bind to *HOX-A* genes to regulate *HOXA* gene expression[14]. Collectively, MA4 and A4M might cooperate through a complex molecular interaction to control *HOX-A* gene regulation[25]. In sum, we describe a functional and molecular cooperation between MA4 and A4M fusions during human hematopoietic development, and demonstrate how hESC-based hematopoietic differentiation represents a promising system to explore the developmental impact of the chimeric proteins resulting from chromosomal translocations, which remains obscure in human leukemia.

AUTHOR CONTRIBUTION: C.B. conceived the study, designed and performed experiments and analyzed data. P.M. conceived the study, designed experiments, analyzed data and wrote the manuscript. F.C.N., X.W., R.V.M., F.G-A., H.R.H., V.A., P.J.R., D.A., L.E., R-T-R., A.A-D., J.dB. performed experiments and analyzed data. I.V., A.B., B.G., and R.M. contributed intellectually and financially

ACKNOWLEDGMENTS. Financial support for this work was obtained from the European Research Council (CoG-2014-646903 and PoC-2018-811220) and the Generalitat de Catalunya (SGR330 and PERIS 2017-2019) to PM, the Spanish Ministry of Economy and Competitiveness (SAF2016-80481-R and SAF2016-76758-R) to PM and IV, the Spanish Association against cancer (AECC-CI-2015) to CB, the Health Institute Carlos III (ISCIII/FEDER, PI17/01028 and PI17/01028) to CB and PJR, the NIHR GOSH BRC and Great Ormond Street Hospital Children's Charity to J.dB, and Bloodwise and Cancer Research UK to BG. RM and PM were also supported by the Deutsche José Carreras Leukämie Stiftung. PM also acknowledges financial support from the Obra Social La Caixa-Fundaciò Josep Carreras. R-T-R is supported by a fellowship from the Spanish Association of Cancer Research (AECC). RV-M is supported by a Torres Quevedo fellowship

by Spanish Ministry of Science and Innovation (PTQ-16-08623). P.M is an investigator of the Spanish Cell Therapy cooperative network (TERCEL).

CONFLICT OF INTEREST DISCLOSURE: The authors have nothing to disclose.

REFERENCES

1. Milne TA. Mouse models of MLL leukemia: recapitulating the human disease. Blood. 2017;129(16):2217-2223.

2. Montes R, Ayllon V, Prieto C, et al. Ligand-independent FLT3 activation does not cooperate with MLL-AF4 to immortalize/transform cord blood CD34+ cells. Leukemia. 2014;28(3):666-674.

3. Stam RW, den Boer ML, Schneider P, et al. Targeting FLT3 in primary MLL-gene-rearranged infant acute lymphoblastic leukemia. Blood. 2005;106(7):2484-2490.

4. Sanjuan-Pla A, Bueno C, Prieto C, et al. Revisiting the biology of infant t(4;11)/MLL-AF4+ B-cell acute lymphoblastic leukemia. Blood. 2015;126(25):2676-2685.

5. Ford AM, Ridge SA, Cabrera ME, et al. In utero rearrangements in the trithorax-related oncogene in infant leukaemias. Nature. 1993;363(6427):358-360.

6. Greaves M. Infection, immune responses and the aetiology of childhood leukaemia. Nat Rev Cancer. 2006;6(3):193-203.

7. Bueno C, Montes R, Catalina P, Rodriguez R, Menendez P. Insights into the cellular origin and etiology of the infant pro-B acute lymphoblastic leukemia with MLL-AF4 rearrangement. Leukemia. 2011;25(3):400-410.

8. Barrett NA, Malouf C, Kapeni C, et al. Mll-AF4 Confers Enhanced Self-Renewal and Lymphoid Potential during a Restricted Window in Development. Cell Rep. 2016;16(4):1039-1054.

9. Bueno C, Ayllon V, Montes R, et al. FLT3 activation cooperates with MLL-AF4 fusion protein to abrogate the hematopoietic specification of human ESCs. Blood. 2013;121(19):3867-3878, S3861-3863.

10. Bueno C, Montes R, Melen GJ, et al. A human ESC model for MLL-AF4 leukemic fusion gene reveals an impaired early hematopoietic-endothelial specification. Cell Res. 2012;22(6):986-1002.

11. Bursen A, Schwabe K, Ruster B, et al. The AF4.MLL fusion protein is capable of inducing ALL in mice without requirement of MLL.AF4. Blood. 2010;115(17):3570-3579.

12. Chen W, Li Q, Hudson WA, et al. A murine Mll-AF4 knock-in model results in lymphoid and myeloid deregulation and hematologic malignancy. Blood. 2006;108(2):669-677.

13. Krivtsov AV, Feng Z, Lemieux ME, et al. H3K79 methylation profiles define murine and human MLL-AF4 leukemias. Cancer Cell. 2008;14(5):355-368.

14. Lin S, Luo RT, Ptasinska A, et al. Instructive Role of MLL-Fusion Proteins Revealed by a Model of t(4;11) Pro-B Acute Lymphoblastic Leukemia. Cancer Cell. 2016;30(5):737-749.

15. Metzler M, Forster A, Pannell R, et al. A conditional model of MLL-AF4 B-cell tumourigenesis using invertor technology. Oncogene. 2006;25(22):3093-3103.

16. Montes R, Ayllon V, Gutierrez-Aranda I, et al. Enforced expression of MLL-AF4 fusion in cord blood CD34+ cells enhances the hematopoietic repopulating cell function and clonogenic potential but is not sufficient to initiate leukemia. Blood. 2011;117(18):4746-4758.

17. Tamai H, Miyake K, Takatori M, et al. Activated K-Ras protein accelerates human MLL/AF4-induced leukemo-lymphomogenicity in a transgenic mouse model. Leukemia. 2011;25(5):888-891.

18. Kowarz E, Burmeister T, Lo Nigro L, et al. Complex MLL rearrangements in t(4;11) leukemia patients with absent AF4.MLL fusion allele. Leukemia. 2007;21(6):1232-1238.

19. Agraz-Doblas A. BC, Bashford-Rogers R., Anindita R., Schneider P., Bardini M., Ballerini P., Cazzaniga G., Moreno T., Revilla C., Gut M., De Lorenzo P., Valsecchi MG, Roberts I, Pieters R, Varela I., Menendez P., Stam R.W. Unravelling the cellular origin and clinical prognosis markers of infant B-cell acute lymphoblastic leukemia using genome-wide analysis. Haematologica. 2018;in press.

20. Trentin L, Giordan M, Dingermann T, et al. Two independent gene signatures in pediatric t(4;11) acute lymphoblastic leukemia patients. Eur J Haematol. 2009;83(5):406-419.

21. Kumar AR, Yao Q, Li Q, Sam TA, Kersey JH. t(4;11) leukemias display addiction to MLL-AF4 but not to AF4-MLL. Leuk Res. 2011;35(3):305-309.

22. Sanders DS, Muntean AG, Hess JL. Significance of AF4-MLL reciprocal fusion in t(4;11) leukemias? Leuk Res. 2011;35(3):299-300.

23. Prieto C, Marschalek R, Kuhn A, et al. The AF4-MLL fusion transiently augments multilineage hematopoietic engraftment but is not sufficient to initiate leukemia in cord blood CD34(+) cells. Oncotarget. 2017;8(47):81936-81941.

24. Rego EM, Pandolfi PP. Reciprocal products of chromosomal translocations in human cancer pathogenesis: key players or innocent bystanders? Trends Mol Med. 2002;8(8):396-405.

25. Wilkinson AC, Ballabio E, Geng H, et al. RUNX1 is a key target in t(4;11) leukemias that contributes to gene activation through an AF4-MLL complex interaction. Cell Rep. 2013;3(1):116-127.

26. Menendez P, Bueno C, Wang L. Human embryonic stem cells: A journey beyond cell replacement therapies. Cytotherapy. 2006;8(6):530-541.

27. Romero-Moya D, Santos-Ocana C, Castano J, et al. Genetic Rescue of Mitochondrial and Skeletal Muscle Impairment in an Induced Pluripotent Stem Cells Model of Coenzyme Q10 Deficiency. Stem Cells. 2017;35(7):1687-1703.

28. Menendez P, Vargas A, Bueno C, et al. Quantitative analysis of bcl-2 expression in normal and leukemic human B-cell differentiation. Leukemia. 2004;18(3):491-498.

29. Ramos-Mejia V, Melen GJ, Sanchez L, et al. Nodal/Activin signaling predicts human pluripotent stem cell lines prone to differentiate toward the hematopoietic lineage. Mol Ther. 2010;18(12):2173-2181.

30. Wang L, Li L, Shojaei F, et al. Endothelial and hematopoietic cell fate of human embryonic stem cells originates from primitive endothelium with hemangioblastic properties. Immunity. 2004;21(1):31-41.

31. Diehl F, Rossig L, Zeiher AM, Dimmeler S, Urbich C. The histone methyltransferase MLL is an upstream regulator of endothelial-cell sprout formation. Blood. 2007;109(4):1472-1478.

32. Hatzipantelis ES, Athanassiou-Metaxa M, Gombakis N, et al. Thrombomodulin and von Willebrand factor: relation to endothelial dysfunction and disease outcome in children with acute lymphoblastic leukemia. Acta Haematol. 2011;125(3):130-135.

33. Menendez P, Catalina P, Rodriguez R, et al. Bone marrow mesenchymal stem cells from infants with MLL-AF4+ acute leukemia harbor and express the MLL-AF4 fusion gene. J Exp Med. 2009;206(13):3131-3141.

34. Ramos-Mejia V, Fernandez AF, Ayllon V, et al. Maintenance of human embryonic stem cells in mesenchymal stem cell-conditioned media augments hematopoietic specification. Stem Cells Dev. 2012;21(9):1549-1558.

35. Sanchez L, Gutierrez-Aranda I, Ligero G, et al. Maintenance of human embryonic stem cells in media conditioned by human mesenchymal stem cells obviates the requirement of exogenous basic fibroblast growth factor supplementation. Tissue Eng Part C Methods. 2012;18(5):387-396.

36. Bueno C, Montes R, Martin L, et al. NG2 antigen is expressed in CD34+ HPCs and plasmacytoid dendritic cell precursors: is NG2 expression in leukemia dependent on the target cell where leukemogenesis is triggered? Leukemia. 2008;22(8):1475-1478.

37. Castano J, Menendez P, Bruzos-Cidon C, et al. Fast and efficient neural conversion of human hematopoietic cells. Stem Cell Reports. 2014;3(6):1118-1131.

38. Munoz-Lopez A, Romero-Moya D, Prieto C, et al. Development Refractoriness of MLL-Rearranged Human B Cell Acute Leukemias to Reprogramming into Pluripotency. Stem Cell Reports. 2016;7(4):602-618.

39. Bueno C, Sardina JL, Di Stefano B, et al. Reprogramming human B cells into induced pluripotent stem cells and its enhancement by C/EBPalpha. Leukemia. 2016;30(3):674-682.

40. Giorgetti A, Castano J, Bueno C, et al. Proinflammatory signals are insufficient to drive definitive hematopoietic specification of human HSCs in vitro. Exp Hematol. 2017;45:85-93 e82.

41. Menendez P, Wang L, Chadwick K, Li L, Bhatia M. Retroviral transduction of hematopoietic cells differentiated from human embryonic stem cell-derived CD45(neg)PFV hemogenic precursors. Mol Ther. 2004;10(6):1109-1120.

42. Bueno C, Roldan M, Anguita E, et al. Bone marrow mesenchymal stem cells from patients with aplastic anemia maintain functional and immune properties and do not contribute to the pathogenesis of the disease. Haematologica. 2014;99(7):1168-1175.

43. Ramos-Mejia V, Navarro-Montero O, Ayllon V, et al. HOXA9 promotes hematopoietic commitment of human embryonic stem cells. Blood. 2014;124(20):3065-3075.

44. Toscano MG, Navarro-Montero O, Ayllon V, et al. SCL/TAL1-mediated transcriptional network enhances megakaryocytic specification of human embryonic stem cells. Mol Ther. 2015;23(1):158-170.

45. Bueno C, Montes R, Menendez P. The ROCK inhibitor Y-27632 negatively affects the expansion/survival of both fresh and cryopreserved cord blood-derived CD34+ hematopoietic progenitor cells: Y-27632 negatively affects the expansion/survival of CD34+HSPCs. Stem Cell Rev. 2010;6(2):215-223.

46. Rubio R, Garcia-Castro J, Gutierrez-Aranda I, et al. Deficiency in p53 but not retinoblastoma induces the transformation of mesenchymal stem cells in vitro and initiates leiomyosarcoma in vivo. Cancer Res. 2010;70(10):4185-4194.

47. Ayllon V, Bueno C, Ramos-Mejia V, et al. The Notch ligand DLL4 specifically marks human hematoendothelial progenitors and regulates their hematopoietic fate. Leukemia. 2015;29(8):1741-1753.

48. Vodyanik MA, Slukvin, II. Hematoendothelial differentiation of human embryonic stem cells. Curr Protoc Cell Biol. 2007;Chapter 23:Unit 23 26.

49. Bueno C, Montes R, de la Cueva T, Gutierrez-Aranda I, Menendez P. Intra-bone marrow transplantation of human CD34(+) cells into NOD/LtSz-scid IL-2rgamma(null) mice permits multilineage engraftment without previous irradiation. Cytotherapy. 2010;12(1):45-49.

50. Gutierrez-Aranda I, Ramos-Mejia V, Bueno C, et al. Human induced pluripotent stem cells develop teratoma more efficiently and faster than human embryonic stem cells regardless the site of injection. Stem Cells. 2010;28(9):1568-1570.

51. Vodyanik MA, Bork JA, Thomson JA, Slukvin, II. Human embryonic stem cell-derived CD34+ cells: efficient production in the coculture with OP9 stromal cells and analysis of lymphohematopoietic potential. Blood. 2005;105(2):617-626.

52. Prieto C, Stam RW, Agraz-Doblas A, et al. Activated KRAS Cooperates with MLL-AF4 to Promote Extramedullary Engraftment and Migration of Cord Blood CD34+ HSPC But Is Insufficient to Initiate Leukemia. Cancer Res. 2016;76(8):2478-2489.

53. Deshpande AJ, Deshpande A, Sinha AU, et al. AF10 regulates progressive H3K79 methylation and HOX gene expression in diverse AML subtypes. Cancer Cell. 2014;26(6):896-908.

54. Guenther MG, Lawton LN, Rozovskaia T, et al. Aberrant chromatin at genes encoding stem cell regulators in human mixed-lineage leukemia. Genes Dev. 2008;22(24):3403-3408.

55. Andersson AK, Ma J, Wang J, et al. The landscape of somatic mutations in infant MLL-rearranged acute lymphoblastic leukemias. Nat Genet. 2015;47(4):330-337.

56. Malouf C, Ottersbach K. The fetal liver lymphoid-primed multipotent progenitor provides the prerequisites for the initiation of t(4;11) MLL-AF4 infant leukemia. Haematologica. 2018.

57. Peters DG, Klucher KM, Perlingeiro RC, et al. Autocrine and paracrine effects of an ES-cell derived, BCR/ABL-transformed hematopoietic cell line that induces leukemia in mice. Oncogene. 2001;20(21):2636-2646.

58. Ji J, Risueno RM, Hong S, et al. Brief report: ectopic expression of NUP98-HOXA10 augments erythroid differentiation of human embryonic stem cells. Stem Cells. 2011;29(4):736-741.

59. Tan YT, Ye L, Xie F, et al. Respecifying human iPSC-derived blood cells into highly engraftable hematopoietic stem and progenitor cells with a single factor. Proc Natl Acad Sci U S A. 2018;115(9):2180-2185.

60. Marschalek R. Mechanisms of leukemogenesis by MLL fusion proteins. Br J Haematol. 2011;152(2):141-154.

61. Boisset JC, van Cappellen W, Andrieu-Soler C, et al. In vivo imaging of haematopoietic cells emerging from the mouse aortic endothelium. Nature. 2010;464(7285):116-120.

62. Ahmad K, Scholz B, Capelo R, et al. AF4 and AF4-MLL mediate transcriptional elongation of 5-lipoxygenase mRNA by 1, 25-dihydroxyvitamin D3. Oncotarget. 2015;6(28):25784-25800.

63. Benedikt A, Baltruschat S, Scholz B, et al. The leukemogenic AF4-MLL fusion protein causes P-TEFb kinase activation and altered epigenetic signatures. Leukemia. 2011;25(1):135-144.

64. Muck F, Bracharz S, Marschalek R. DDX6 transfers P-TEFb kinase to the AF4/AF4N (AFF1) super elongation complex. Am J Blood Res. 2016;6(3):28-45.

65. Driessen EM, van Roon EH, Spijkers-Hagelstein JA, et al. Frequencies and prognostic impact of RAS mutations in MLL-rearranged acute lymphoblastic leukemia in infants. Haematologica. 2013;98(6):937-944.

66. Kuhn A, Loscher D, Marschalek R. The IRX1/HOXA connection: insights into a novel t(4;11)- specific cancer mechanism. Oncotarget. 2016;7(23):35341-35352.

FIGURE LEGENDS

Figure 1. Characterization of transgenic human ESCs expressing the reciprocal fusion A4M together with MA4. (A) RNA-seq and qRT-PCR validation revealed that ~45% (11/25) of the patients with t(4;11)+ B-ALL do not express the reciprocal fusion A4M[18]. (B) *Left*, Phase-contrast morphology of representative colonies from each transgenic hESC line. *Right*, RT-PCR confirming expression of both fusions in undifferentiated hESCs. (C) qRT-PCR expression of the pluripotency genes *OCT4, SOX2, NANOG, CRIPTO*, and *DNMT3B*. (D) Representative FACS data confirming expression of the pluripotency surface makers SSEA-3, SSEA-4, TRA-1-60, and TRA-1-81.

Figure 2. A4M cooperates with MA4 to accelerate human ESC/EB specification towards HEPs and subsequent hematopoietic differentiation. (A) Schematic of EB hematopoietic differentiation of hESCs and end-point analyses. (B) *Upper left,* specification into HEPs ($CD31^+CD34^+CD45^-$) is accelerated in double fusion-expressing hESCs. Subsequent differentiation of HEPs into hematopoietic progenitors (*upper right*) and mature $CD45^+$ blood cells (*bottom left*) is enhanced in double fusion-expressing HEPs. *Bottom right*, CFU read-out and scoring (pie charts) confirming an accelerated and enhanced hematopoietic progenitor potential from double fusion-expressing blood derivatives. (C) RT-PCR confirming stable expression of MA4 and A4M upon EB differentiation. (D) Neither MA4- nor double fusion-expressing blood derivatives display *in vivo* hematopoietic engraftment potential in irradiated NSG mice. Data are presented as mean±SEM from at least three independent experiments. *$p<0.05$.

Figure 3. Co-expression of MA4 and A4M enhances hematopoietic differentiation of human ESCs in OP9 co-culture. (A) Experimental design of OP9-based hESC differentiation towards HEPs and further hematopoietic commitment of HEPs maintained in either liquid culture for 16 days or in MS5 co-culture for 30 days. (B) Frequency of total CD45+ blood cells after 9 days in OP9 co-culture. (C,D) CD45-CD31+CD34+

HEPs were FACS-purified at day 9 of OP9 co-culture and allowed to differentiate into CD45+ cells in liquid culture (C) or in MS5 co-culture (D). Data represent mean±SEM from independent experiments.

Figure 4. Enhanced endothelial cell fate from HEPs co-expressing MA4 and A4M. (A) Scheme of HEPs endothelial differentiation and phenotypic characterization. (B) FACS-sorted HEPs from day 9 human ESC-OP9 co-cultures were cultured in EGM2 medium for 5 days and analyzed by immunofluorescence for VE-cadherin, eNOS and vWF. (C) *Top*, Endothelial-like structures were identified and quantified based on VE-cadherin staining (white dotted-lined areas in B, *top panel*). *Bottom*, Frequency of $CD45^{-}CD31^{+}CD144^{+}$ endothelial cells quantified by flow cytometry. (D) *In vivo* endothelial engraftment potential ($HLA.ABC^{+}CD31^{+}CD144^{+}CD45^{-}$) analyzed in bone marrow of NSG mice 8 weeks after transplantation of HEPs. Data presented as mean±SEM from 5 independent experiments. *p<0.05.

Figure 5. Co-expression of MA4 and A4M significantly enhances the emergence of both endothelial and hemogenic HEPs. (A) Representative flow cytometry analysis of HEPs with hemogenic ($CD45^{-}CD31^{+}CD43^{+}CD34^{dim/+}$) and endothelial ($CD45^{-}CD31^{+}CD43^{-}CD34^{++}$) potential. (B,C) A4M cooperates with MA4 to boost the emergence of both endothelial (B) and hemogenic (C) HEPs. Data presented as mean±SEM from 3 independent experiments. (D) Expression of *RUNX1c* and *Ve-Cad* in hemogenic and endothelial HEPs. * p<0.05

Figure 6: Transcriptional transition towards a hematopoietic/endothelial gene signature in double fusion-expressing HEPs. (A) Heatmap representation of hierarchical clustering of genes differentially expressed between EV-, single fusions- and double fusion-expressing HEPs. Each column represents a technical replicate from three independent experiments. (B,C) Statistically significant functional categories (B) and cancer/leukemia-associated biofunctions (C) identified using IPA on genes differentially expressed

in single fusions-, and double fusion-expressing HEPs relative to EV. They are ranked by z-score. Functional categories associated with “hematological system development and function” and “cardiovascular system development” are shown in bold. All significant biofunctions are associated with blood cell differentiation, homeostasis and migration/movement.

Figure 7: H3K79 methylation profiles at genomic loci of MLL targets in MA4-, A4M- and double fusion-expressing human ESC-derived blood derivatives. (A) GO enrichment of differential H3K79me3 peaks specific for double fusion-expressing cells. (B-C) Representative profiles for ChIP-seq using anti-H3K79me^3 antibody at genomic regions of typical non-HOXA (B) and *HOXA* MLL targets (C).

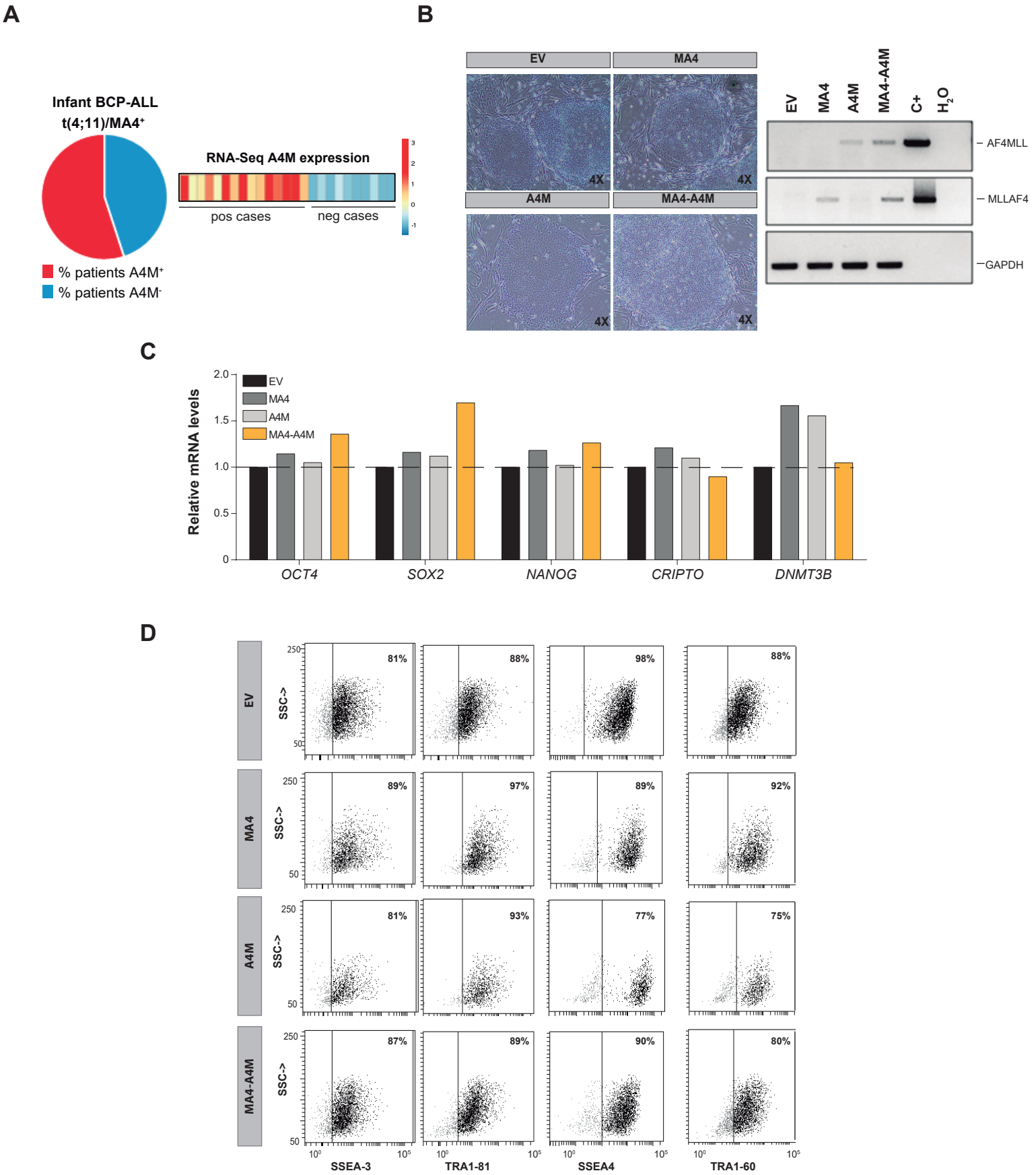
A
Infant BCP-ALL
t(4;11)/MA4+
% patients A4M+
% patients A4M-
RNA-Seq A4M expression
pos cases
neg cases
B
EV
MA4
A4M
MA4-A4M
4X
EV
MA4
A4M
MA4-A4M
C+
H2O
AF4MLL
MLLAF4
GAPDH
C
Relative mRNA levels
EV
MA4
A4M
MA4-A4M
OCT4
SOX2
NANOG
CRIPTO
DNMT3B
D
EV
MA4
A4M
MA4-A4M
SSC->
81%
88%
98%
88%
89%
97%
89%
92%
81%
93%
77%
75%
87%
89%
90%
80%
SSEA-3
TRA1-81
SSEA4
TRA1-60

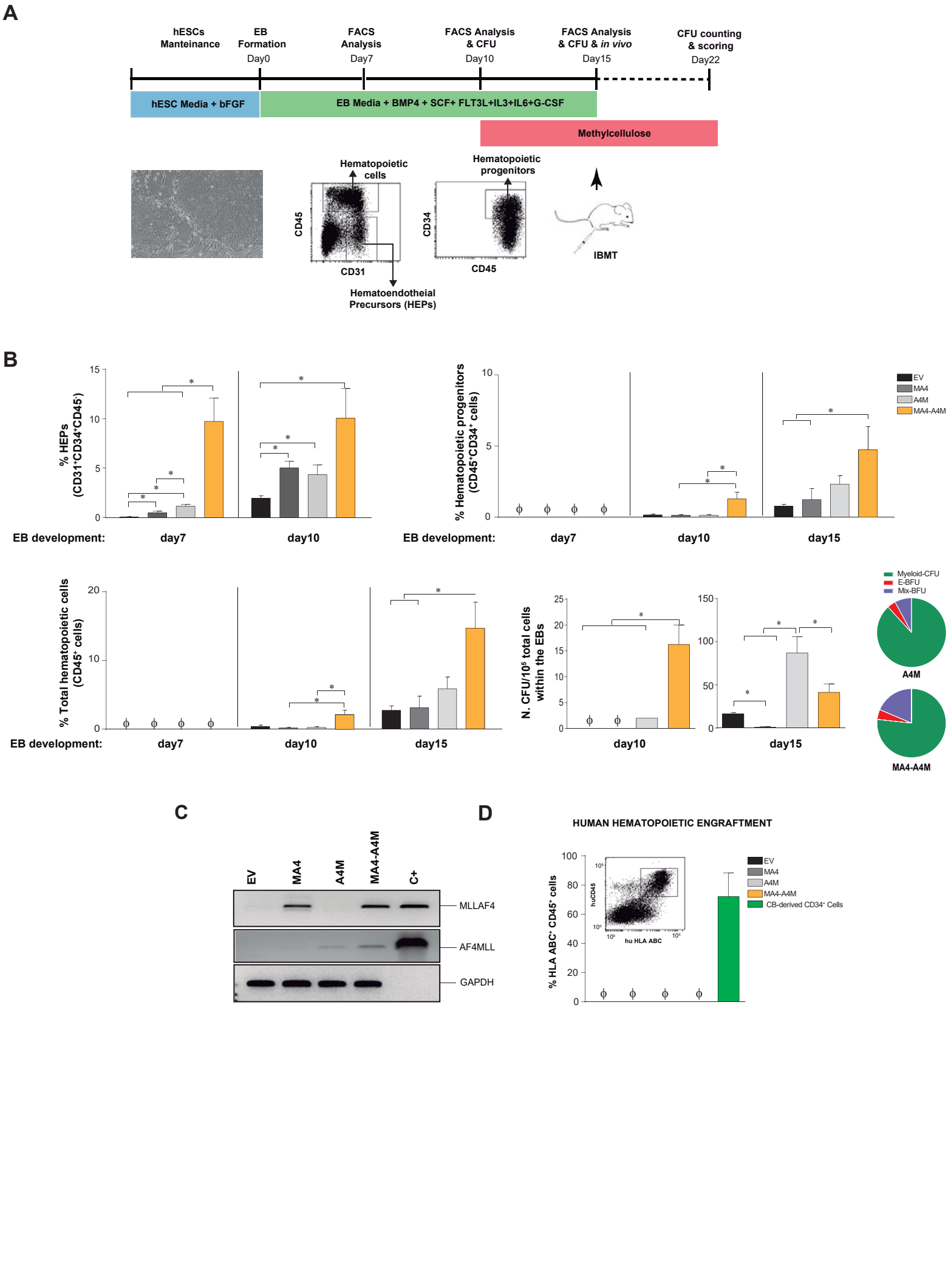
A
hESCs Manteinance
EB Formation
Day0
FACS Analysis
Day7
FACS Analysis & CFU
Day10
FACS Analysis & CFU & in vivo
Day15
CFU counting & scoring
Day22
hESC Media + bFGF
EB Media + BMP4 + SCF+ FLT3L+IL3+IL6+G-CSF
Methylcellulose
Hematopoietic cells
CD45
CD31
Hematoendotheial Precursors (HEPs)
Hematopoietic progenitors
CD34
CD45
IBMT
B
% HEPs (CD31+CD34+CD45-)
EB development:
day7
day10
% Hematopoietic progenitors (CD45+CD34+ cells)
EV
MA4
A4M
MA4-A4M
day15
% Total hematopoietic cells (CD45+ cells)
N. CFU/10^5 total cells within the EBs
Myeloid-CFU
E-BFU
Mix-BFU
A4M
MA4-A4M
C
EV
MA4
A4M
MA4-A4M
C+
MLLAF4
AF4MLL
GAPDH
D
HUMAN HEMATOPOIETIC ENGRAFTMENT
% HLA ABC+ CD45+ cells
huCD45
hu HLA ABC
CB-derived CD34+ Cells

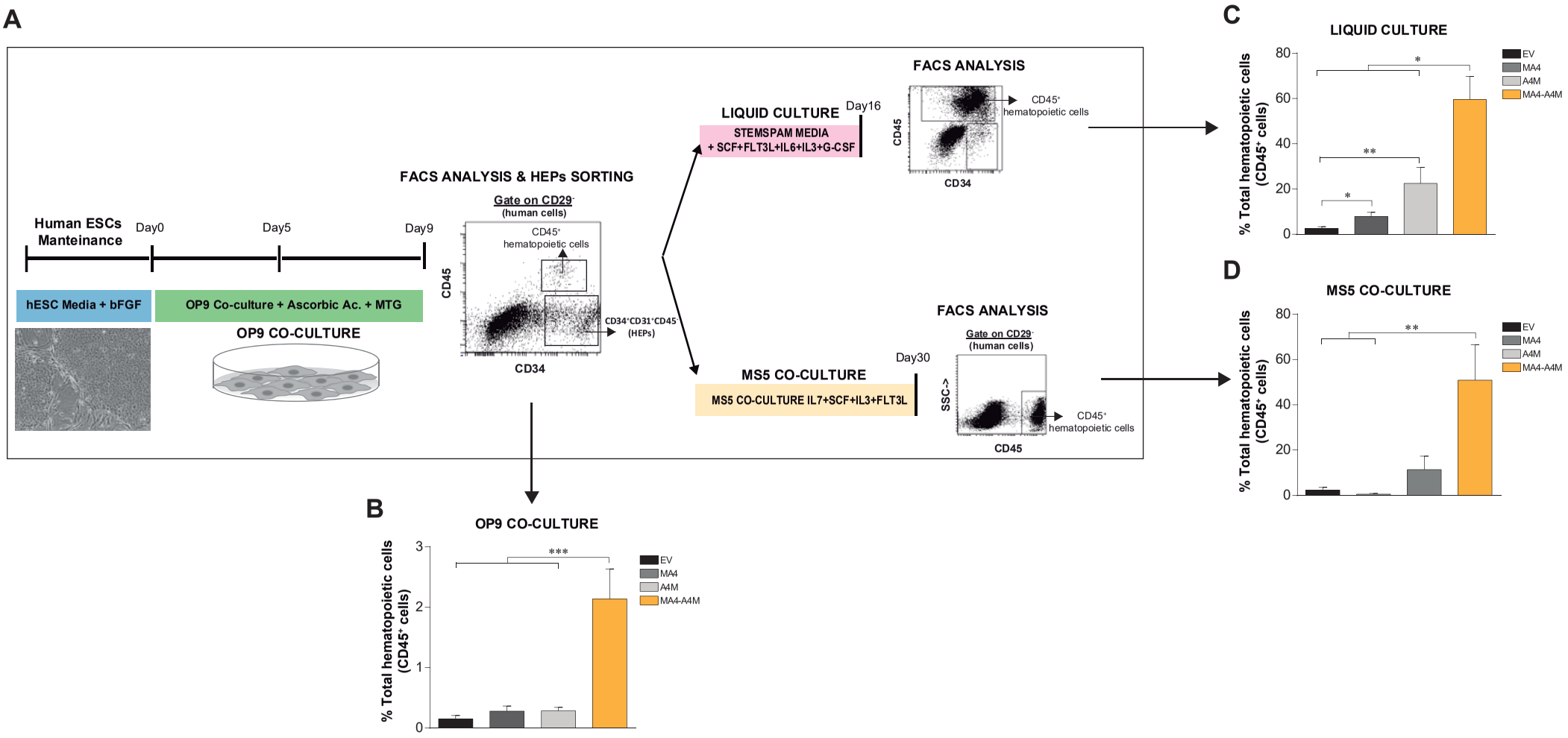
A
Human ESCs Manteinance
Day0
Day5
Day9
hESC Media + bFGF
OP9 Co-culture + Ascorbic Ac. + MTG
OP9 CO-CULTURE
FACS ANALYSIS & HEPs SORTING
Gate on CD29-
(human cells)
CD45+ hematopoietic cells
CD34+CD31+CD45- (HEPs)
CD45
CD34
LIQUID CULTURE
Day16
STEMSPAM MEDIA
+ SCF+FLT3L+IL6+IL3+G-CSF
FACS ANALYSIS
CD45+ hematopoietic cells
CD45
CD34
MS5 CO-CULTURE
Day30
MS5 CO-CULTURE IL7+SCF+IL3+FLT3L
FACS ANALYSIS
Gate on CD29-
(human cells)
SSC->
CD45+ hematopoietic cells
CD45
B
OP9 CO-CULTURE
% Total hematopoietic cells (CD45+ cells)
***
EV
MA4
A4M
MA4-A4M
C
LIQUID CULTURE
% Total hematopoietic cells (CD45+ cells)
*
**
*
EV
MA4
A4M
MA4-A4M
D
MS5 CO-CULTURE
% Total hematopoietic cells (CD45+ cells)
**
EV
MA4
A4M
MA4-A4M

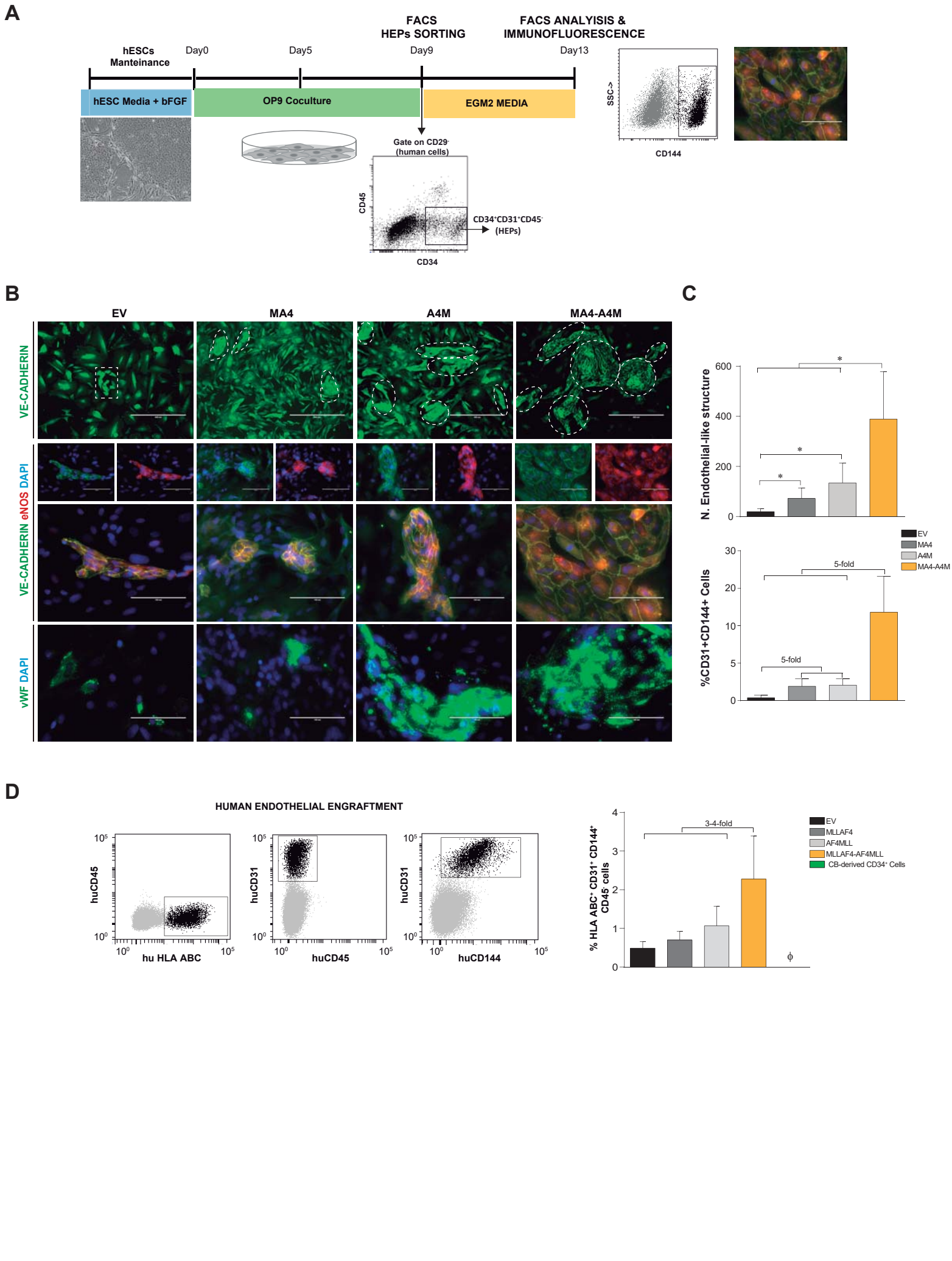
A
FACS HEPs SORTING
FACS ANALYISIS & IMMUNOFLUORESCENCE
hESCs Manteinance
Day0
Day5
Day9
Day13
hESC Media + bFGF
OP9 Coculture
EGM2 MEDIA
Gate on CD29- (human cells)
CD45
CD34
CD34+CD31+CD45- (HEPs)
SSC->
CD144
B
EV
MA4
A4M
MA4-A4M
VE-CADHERIN
VE-CADHERIN eNOS DAPI
vWF DAPI
C
N. Endothelial-like structure
600
400
200
0
*
*
*
%CD31+CD144+ Cells
30
20
10
5
0
5-fold
5-fold
EV
MA4
A4M
MA4-A4M
D
HUMAN ENDOTHELIAL ENGRAFTMENT
huCD45
hu HLA ABC
huCD31
huCD45
huCD31
huCD144
% HLA ABC+ CD31+ CD144+ CD45- cells
4
3
2
1
0
3-4-fold
ϕ
EV
MLLAF4
AF4MLL
MLLAF4-AF4MLL
CB-derived CD34+ Cells

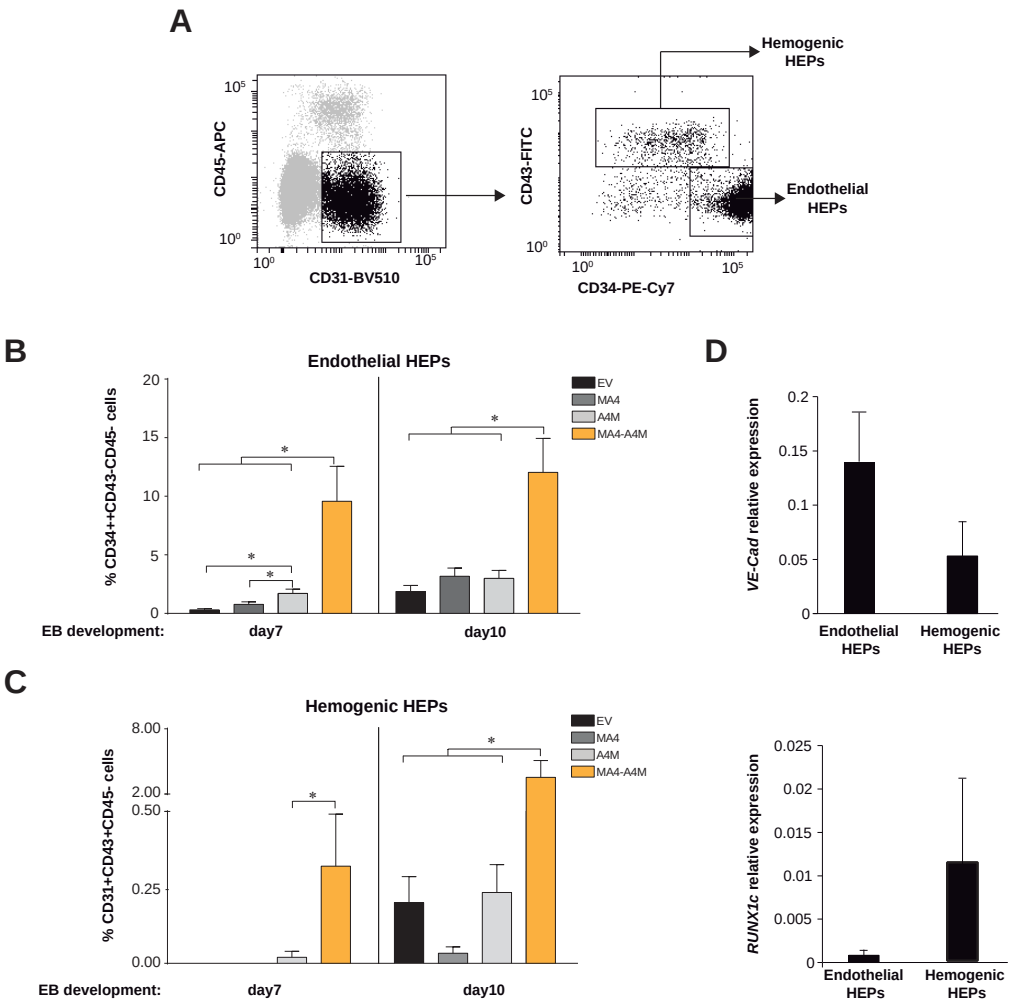
A
CD45-APC
CD31-BV510
CD43-FITC
CD34-PE-Cy7
Hemogenic HEPs
Endothelial HEPs
B
Endothelial HEPs
% CD34++CD43-CD45- cells
EV
MA4
A4M
MA4-A4M
EB development:
day7
day10
C
Hemogenic HEPs
% CD31+CD43+CD45- cells
D
VE-Cad relative expression
RUNX1c relative expression
Endothelial HEPs
Hemogenic HEPs

A

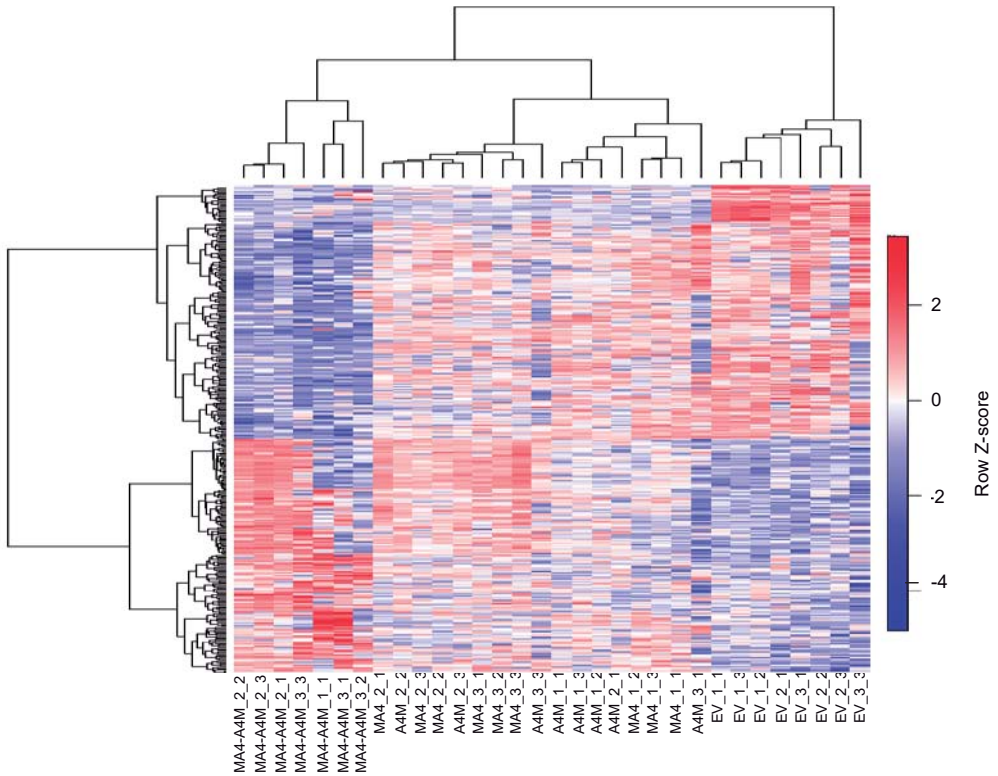

B

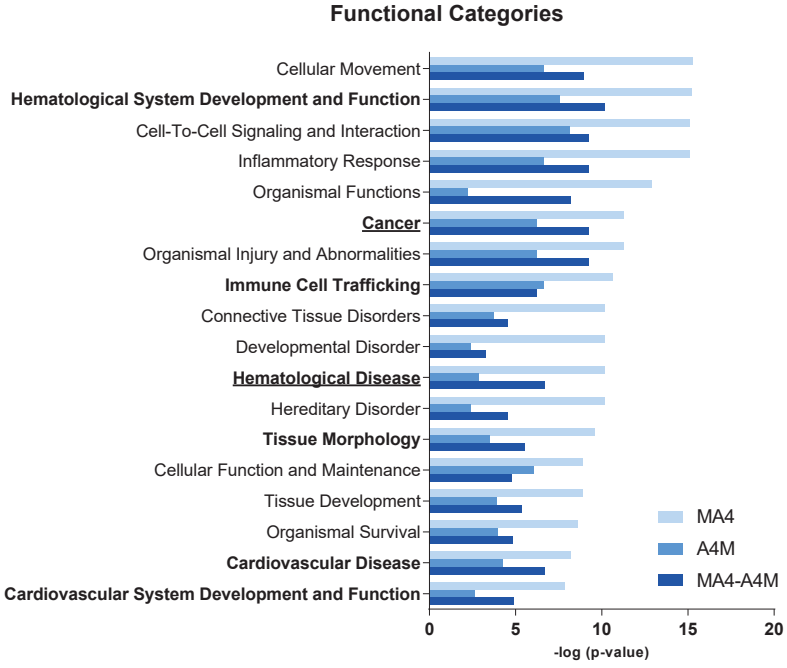

C

Cancer Functions

	MA4	A4M	MA4-A4M
Lymphatic system tumor	-0.313		2.025
Lymphatic cancer	-0.313		2.025
Lymphocytic neoplasm	-0.313		2.025
Lymphoid cancer	-0.313		2.025
Neoplasia of leukocytes	-0.313		2.025
Hematologic cancer of cells	-0.313		2.016
Lymphoma	-0.313		1.977
Hematologic cancer	-0.537		1.886
Lymphoreticular neoplasm	-0.014		1.854
Neoplasia of cells	-1.116		1.498
Hematopoietic neoplasm	-0.788		1.472
Carcinoma	-1.526	1.464	-0.445
Non-hematological neoplasm	-1.19	1.662	-0.45
Nonhematologic malignantneoplasm	-0.859	1.714	-0.61
Digestive organ tumor	-1.541	-1.231	-1.026

Haematological Disease Functions

	MA4	A4M	MA4-A4M
Thrombus	1.714		0.23
Formation of thrombus	1.067		-0.277
Hematologic cancer of cells	-0.313		2.016
Lymphocytic cancer	-0.313		2.025
Lymphocytic neoplasm	-0.313		2.025
Lymphoid cancer	-0.313		2.025
Lymphoma	-0.313		1.977
Lymphoproliferative disorder	-0.313		2.025
Neoplasia of leukocyte	-0.313		2.025
Hematologic cancer	-0.537		1.886
Hematopoietic neoplasm	-0.788		1.472
Cytopenia	-2.66		
Thrombocytopenia	-2.831		
Hemorrhagic disease	-3.137		

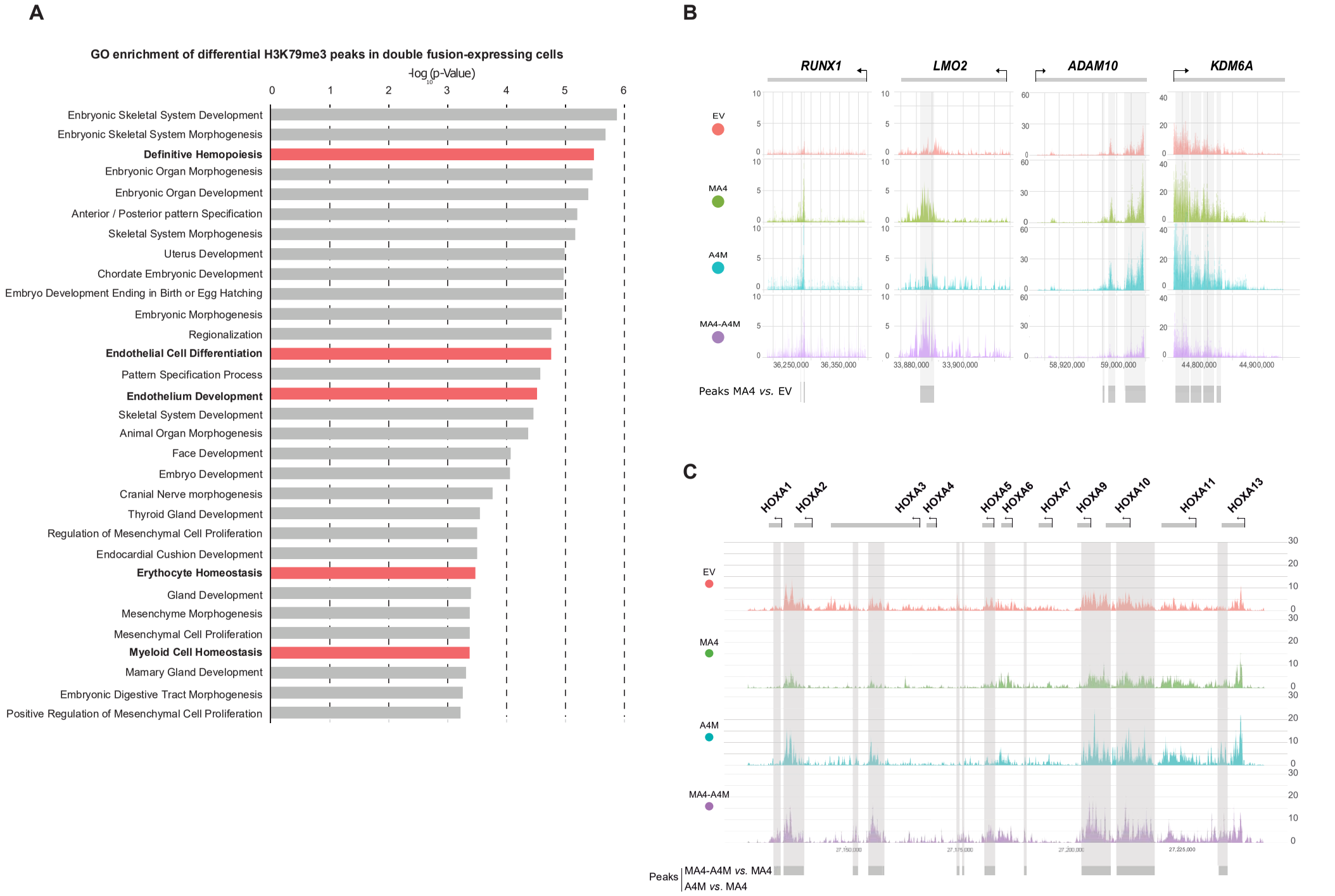
A
GO enrichment of differential H3K79me3 peaks in double fusion-expressing cells
-log10(p-Value)
0
1
2
3
4
5
6
Enbryonic Skeletal System Development
Enbryonic Skeletal System Morphogenesis
Definitive Hemopoiesis
Enbryonic Organ Morphogenesis
Enbryonic Organ Development
Anterior / Posterior pattern Specification
Skeletal System Morphogenesis
Uterus Development
Chordate Embryonic Development
Embryo Development Ending in Birth or Egg Hatching
Embryonic Morphogenesis
Regionalization
Endothelial Cell Differentiation
Pattern Specification Process
Endothelium Development
Skeletal System Development
Animal Organ Morphogenesis
Face Development
Embryo Development
Cranial Nerve morphogenesis
Thyroid Gland Development
Regulation of Mesenchymal Cell Proliferation
Endocardial Cushion Development
Erythocyte Homeostasis
Gland Development
Mesenchyme Morphogenesis
Mesenchymal Cell Proliferation
Myeloid Cell Homeostasis
Mamary Gland Development
Embryonic Digestive Tract Morphogenesis
Positive Regulation of Mesenchymal Cell Proliferation
B
RUNX1
LMO2
ADAM10
KDM6A
EV
MA4
A4M
MA4-A4M
36,250,000
36,350,000
33,880,000
33,900,000
58,920,000
59,000,000
44,800,000
44,900,000
Peaks MA4 vs. EV
C
HOXA1
HOXA2
HOXA3
HOXA4
HOXA5
HOXA6
HOXA7
HOXA9
HOXA10
HOXA11
HOXA13
EV
MA4
A4M
MA4-A4M
Peaks
MA4-A4M vs. MA4
A4M vs. MA4

Bueno C *et al.* Figure S1

A

AF4-MLL (8739 bp)

Red: AF4 exon 1-3

Blue: MLL exon 10 to 36

ATG :Start Codon

TAA :Stop Codon

ATGGCAGCCCAGTCAAGTTTGTACAATGACGACAGAAACCTGCTTCGAATTAGAGAGAAGGAA
AGACGCAACCAGGAAGCCCACCAAGAGAAAGAGGCATTTCCTGAAAAGATTCCCCTTTTTGGA
GAGCCCTACAAGACAGCAAAAGGTGATGAGCTGTCTAGTCGAATACAGAACATGTTGGGAAAC
TACGAAGAAGTGAAGGAGTTCCTTAGTACTAAGTCTCACACTCATCGCCTGGATGCTTCTGAAA
ATAGGTTGGGAAAGCCGAAATATCCTTTAATTCCTGACAAAGGGAGCAGCATTCCATCCAGCT
CCTTCCACACTAGTGTCCACCACCAGTCCATTCACACTCCTGCGTCTGGACCACTTTCTGTTGG
CAACATTAGCCACAATCCAAAGATGGCGCAGCCAAGAACTGAACCAATGCCAAGTCTCCATGC
CAAAAGCTGCGGCCCACCGGACAGCCAGCACCTGACCCAGGATCGCCTTGGTCAGGAGGGG
TTCGGCTCTAGTCATCACAAGAAAGGTGACCGAAGAGCTGACGGAGACCACTGTGCTTCGGT
GACAGATTCGGCTCCAGAGAGGGAGCTTTCTCCCTTAATCTCTTTGCCTTCCCCAGTTCCCCC
TTTGTCACCTATACATTCCAACCAGCAAACTCTTCCCCGGACGCAAGGAAGCAGCAAGGTTCA
TGGCAGCAGCAATAACAGTAAAGGCTATTGCCCAGCCAAATCTCCCAAGGACCTAGCAGTGAA
AGTCCATGATAAAGAGACCCCTCAAGACAGTTTGGTGGCCCCTGCCCAGCCGCCTTCTCAGAC
ATTTCCACCTCCCTCCCTCCCCTCAAAAAGTGTTGCAATGCAGCAGAAGCCCACGGCTTATGT
CCGGCCCATGGATGGTCAAGATCAGGCCCCTAGTGAATCCCCTGAACTGAAACCACTGCCGG
AGGACTATCGACAGCAGACCTTTGAAAAAACAGACTTGAAAGTGCCTGCCAAAGCCAAGCTCA
CCAAACTGAAGATGCCTTCTCAGTCAGTTGAGGAGGATTGTGAAGCAGAAAATGTGTGGGAGA
TGGGAGGCTTAGGAATCTTGACTTCTGTTCCTATAACACCCAGGGTGGTTTGCTTTCTCTGTGC
CAGTAGTGGGCATGTAGAGTTTGTGTATTGCCAAGTCTGTTGTGAGCCCTTCCACAAGTTTTGT
TTAGAGGAGAACGAGCGCCCTCTGGAGGACCAGCTGGAAAATTGGTGTTGTCGTCGTTGCAA
ATTCTGTCACGTTTGTGGAAGGCAACATCAGGCTACAAAGCAGCTGCTGGAGTGTAATAAGTG
CCGAAACAGCTATCACCCTGAGTGCCTGGGACCAAACTACCCCACCAAACCCACAAAGAAGAA
GAAAGTCTGGATCTGTACCAAGTGTGTTCGCTGTAAGAGCTGTGGATCCACAACTCCAGGCAA
AGGGTGGGATGCACAGTGGTCTCATGATTTCTCACTGTGTCATGATTGCGCCAAGCTCTTTGC
TAAAGGAAACTTCTGCCCTCTCTGTGACAAATGTTATGATGATGATGACTATGAGAGTAAGATG
ATGCAATGTGGAAAGTGTGATCGCTGGGTCCATTCCAAATGTGAGAATCTTTCAGGTACAGAA
GATGAGATGTATGAGATTCTATCTAATCTGCCAGAAAGTGTGGCCTACACTTGTGTGAACTGTA
CTGAGCGGCACCCTGCAGAGTGGCGACTGGCCCTTGAAAAAGAGCTGCAGATTTCTCTGAAG
CAAGTTCTGACAGCTTTGTTGAATTCTCGGACTACCAGCCATTTGCTACGCTACCGGCAGGCT
GCCAAGCCTCCAGACTTAAATCCCGAGACAGAGGAGAGTATACCTTCCCGCAGCTCCCCCGA
AGGACCTGATCCACCAGTTCTTACTGAGGTCAGCAAACAGGATGATCAGCAGCCTTTAGATCT
AGAAGGAGTCAAGAGGAAGATGGACCAAGGGAATTACACATCTGTGTTGGAGTTCAGTGATGA
TATTGTGAAGATCATTCAAGCAGCCATTAATTCAGATGGAGGACAGCCAGAAATTAAAAAAGCC
AACAGCATGGTCAAGTCCTTCTTCATTCGGCAAATGGAACGTGTTTTTCCATGGTTCAGTGTCA
AAAAGTCCAGGTTTTGGGAGCCAAATAAAGTATCAAGCAACAGTGGGATGTTACCAAACGCAG
TGCTTCCACCTTCACTTGACCATAATTATGCTCAGTGGCAGGAGCGAGAGGAAAACAGCCACA
CTGAGCAGCCTCCTTTAATGAAGAAAATCATTCCAGCTCCCAAACCCAAAGGTCCTGGAGAAC
CAGACTCACCAACTCCTCTGCATCCTCCTACACCACCAATTTTGAGTACTGATAGGAGTCGAGA
AGACAGTCCAGAGCTGAACCCACCCCCAGGCATAGAAGACAATAGACAGTGTGCGTTATGTTT
GACTTATGGTGATGACAGTGCTAATGATGCTGGTCGTTTACTATATATTGGCCAAAATGAGTGG

ACACATGTAAATTGTGCTTTGTGGTCAGCGGAAGTGTTTGAAGATGATGACGGATCACTAAAGA
ATGTGCATATGGCTGTGATCAGGGGCAAGCAGCTGAGATGTGAATTCTGCCAAAAGCCAGGA
GCCACCGTGGGTTGCTGTCTCACATCCTGCACCAGCAACTATCACTTCATGTGTTCCCGAGCC
AAGAACTGTGTCTTTCTGGATGATAAAAAAGTATATTGCCAACGACATCGGGATTTGATCAAAG
GCGAAGTGGTTCCTGAGAATGGATTTGAAGTTTTCAGAAGAGTGTTTGTGGACTTTGAAGGAAT
CAGCTTGAGAAGGAAGTTTCTCAATGGCTTGGAACCAGAAAATATCCACATGATGATTGGGTCT
ATGACAATCGACTGCTTAGGAATTCTAAATGATCTCTCCGACTGTGAAGATAAGCTCTTTCCTAT
TGGATATCAGTGTTCCAGGGTATACTGGAGCACCACAGATGCTCGCAAGCGCTGTGTATATAC
ATGCAAGATAGTGGAGTGCCGTCCTCCAGTCGTAGAGCCGGATATCAACAGCACTGTTGAACA
TGATGAAAACAGGACCATTGCCCATAGTCCAACATCTTTTACAGAAAGTTCATCAAAAGAGAGT
CAAAACACAGCTGAAATTATAAGTCCTCCATCACCAGACCGACCTCCTCATTCACAAACCTCTG
GCTCCTGTTATTATCATGTCATCTCAAAGGTCCCCAGGATTCGAACACCCAGTTATTCTCCAAC
ACAGAGATCCCCTGGCTGTCGACCGTTGCCTTCTGCAGGAAGTCCTACCCCAACCACTCATGA
AATAGTCACAGTAGGTGATCCTTTACTCTCCTCTGGACTTCGAAGCATTGGCTCCAGGCGTCA
CAGTACCTCTTCCTTATCACCCCAGCGGTCCAAACTCCGGATAATGTCTCCAATGAGAACTGG
GAATACTTACTCTAGGAATAATGTTTCCTCAGTCTCCACCACCGGGACCGCTACTGATCTTGAA
TCAAGTGCCAAAGTAGTTGATCATGTCTTAGGGCCACTGAATTCAAGTACTAGTTTAGGGCAAA
ACACTTCCACCTCTTCAAATTTGCAAAGGACAGTGGTTACTGTAGGCAATAAAAACAGTCACTT
GGATGGATCTTCATCTTCAGAAATGAAGCAGTCCAGTGCTTCAGACTTGGTGTCCAAGAGCTC
CTCTTTAAAGGGAGAGAAGACCAAAGTGCTGAGTTCCAAGAGCTCAGAGGGATCTGCACATAA
TGTGGCTTACCCTGGAATTCCTAAACTGGCCCCACAGGTTCATAACACAACATCTAGAGAACTG
AATGTTAGTAAAATCGGCTCCTTTGCTGAACCCTCTTCAGTGTCGTTTTCTTCTAAAGAGGCCC
TCTCCTTCCCACACCTCCATTTGAGAGGGCAAAGGAATGATCGAGACCAACACACAGATTCTA
CCCAATCAGCAAACTCCTCTCCAGATGAAGATACTGAAGTCAAAACCTTGAAGCTATCTGGAAT
GAGCAACAGATCATCCATTATCAACGAACATATGGGATCTAGTTCCAGAGATAGGAGACAGAA
AGGGAAAAAATCCTGTAAAGAAACTTTCAAAGAAAAGCATTCCAGTAAATCTTTTTTGGAACCTG
GTCAGGTGACAACTGGTGAGGAAGGAAACTTGAAGCCAGAGTTTATGGATGAGGTTTTGACTC
CTGAGTATATGGGCCAACGACCATGTAACAATGTTTCTTCTGATAAGATTGGTGATAAAGGCCT
TTCTATGCCAGGAGTCCCCAAAGCTCCACCCATGCAAGTAGAAGGATCTGCCAAGGAATTACA
GGCACCACGGAAACGCACAGTCAAAGTGACACTGACACCTCTAAAAATGGAAAATGAGAGTCA
ATCCAAAAATGCCCTGAAAGAAAGTAGTCCTGCTTCCCCTTTGCAAATAGAGTCAACATCTCCC
ACAGAACCAATTTCAGCCTCTGAAAATCCAGGAGATGGTCCAGTGGCCCAACCAAGCCCCAAT
AATACCTCATGCCAGGATTCTCAAAGTAACAACTATCAGAATCTTCCAGTACAGGACAGAAACC
TAATGCTTCCAGATGGCCCCAAACCTCAGGAGGATGGCTCTTTTAAAAGGAGGTATCCCCGTC
GCAGTGCCCGTGCACGTTCTAACATGTTTTTTGGGCTTACCCCACTCTATGGAGTAAGATCCTA
TGGTGAAGAAGACATTCCATTCTACAGCAGCTCAACTGGGAAGAAGCGAGGCAAGAGATCAGC
TGAAGGACAGGTGGATGGGGCCGATGACTTAAGCACTTCAGATGAAGACGACTTATACTATTA
CAACTTCACTAGAACAGTGATTTCTTCAGGTGGAGAGGAACGACTGGCATCCCATAATTTATTT
CGGGAGGAGGAACAGTGTGATCTTCCAAAAATCTCACAGTTGGATGGTGTTGATGATGGGACA
GAGAGTGATACTAGTGTCACAGCCACAACAAGGAAAAGCAGCCAGATTCCAAAAAGAAATGGT
AAAGAAAATGGAACAGAGAACTTAAAGATTGATAGACCTGAAGATGCTGGGGAGAAAGAACAT
GTCACTAAGAGTTCTGTTGGCCACAAAAATGAGCCAAAGATGGATAACTGCCATTCTGTAAGCA
GAGTTAAAACACAGGGACAAGATTCCTTGGAAGCTCAGCTCAGCTCATTGGAGTCAAGCCGCA
GAGTCCACACAAGTACCCCCTCCGACAAAAATTTACTGGACACCTATAATACTGAGCTCCTGAA
ATCAGATTCAGACAATAACAACAGTGATGACTGTGGGAATATCCTGCCTTCAGACATTATGGAC
TTTGTACTAAAGAATACTCCATCCATGCAGGCTTTGGGTGAGAGCCCAGAGTCATCTTCATCAG
AACTCCTGAATCTTGGTGAAGGATTGGGTCTTGACAGTAATCGTGAAAAAGACATGGGTCTTTT
TGAAGTATTTTCTCAGCAGCTGCCTACAACAGAACCTGTGGATAGTAGTGTCTCTTCCTCTATC
TCAGCAGAGGAACAGTTTGAGTTGCCTCTAGAGCTACCATCTGATCTGTCTGTCTTGACCACC
CGGAGTCCCACTGTCCCCAGCCAGAATCCCAGTAGACTAGCTGTTATCTCAGACTCAGGGGA
GAAGAGAGTAACCATCACAGAAAAATCTGTAGCCTCCTCTGAAAGTGACCCAGCACTGCTGAG
CCCAGGAGTAGATCCAACTCCTGAAGGCCACATGACTCCTGATCATTTTATCCAAGGACACAT

GGATGCAGACCACATCTCTAGCCCTCCTTGTGGTTCAGTAGAGCAAGGTCATGGCAACAATCA
GGATTTAACTAGGAACAGTAGCACCCCTGGCCTTCAGGTACCTGTTTCCCCAACTGTTCCCAT
CCAGAACCAGAAGTATGTGCCCAATTCTACTGATAGTCCTGGCCCGTCTCAGATTTCCAATGCA
GCTGTCCAGACCACTCCACCCCACCTGAAGCCAGCCACTGAGAAACTCATAGTTGTTAACCAG
AACATGCAGCCACTTTATGTTCTCCAAACTCTTCCAAATGGAGTGACCCAAAAAATCCAATTGA
CCTCTTCTGTTAGTTCTACACCCAGTGTGATGGAGACAAATACTTCAGTATTGGGACCCATGGG
AGGTGGTCTCACCCTTACCACAGGACTAAATCCAAGCTTGCCAACTTCTCAATCTTTGTTCCCT
TCTGCTAGCAAAGGATTGCTACCCATGTCTCATCACCAGCACTTACATTCCTTCCCTGCAGCTA
CTCAAAGTAGTTTCCCACCAAACATCAGCAATCCTCCTTCAGGCCTGCTTATTGGGGTTCAGCC
TCCTCCGGATCCCCAACTTTTGGTTTCAGAATCCAGCCAGAGGACAGACCTCAGTACCACAGT
AGCCACTCCATCCTCTGGACTCAAGAAAAGACCCATATCTCGTCTACAGACCCGAAAGAATAAA
AAACTTGCTCCCTCTAGTACCCCTTCAAACATTGCCCCTTCTGATGTGGTTTCTAATATGACATT
GATTAACTTCACACCCTCCCAGCTTCCTAATCATCCAAGTCTGTTAGATTTGGGGTCACTTAATA
CTTCATCTCACCGAACTGTCCCCAACATCATAAAAAGATCTAAATCTAGCATCATGTATTTTGAA
CCGGCACCCCTGTTACCACAGAGTGTGGGAGGAACTGCTGCCACAGCGGCAGGCACATCAAC
AATAAGCCAGGATACTAGCCACCTCACATCAGGGTCTGTGTCTGGCTTGGCATCCAGTTCCTC
TGTCTTGAATGTTGTATCCATGCAAACTACCACAACCCCTACAAGTAGTGCGTCAGTTCCAGGA
CACGTCACCTTAACCAACCCAAGGTTGCTTGGTACCCCAGATATTGGCTCAATAAGCAATCTTT
TAATCAAAGCTAGCCAGCAGAGCCTGGGGATTCAGGACCAGCCTGTGGCTTTACCGCCAAGTT
CAGGAATGTTTCCACAACTGGGGACATCACAGACCCCCTCTACTGCTGCAATAACAGCGGCAT
CTAGCATCTGTGTGCTCCCCTCCACTCAGACTACGGGCATAACAGCCGCTTCACCTTCTGGGG
AAGCAGACGAACACTATCAGCTTCAGCATGTGAACCAGCTCCTTGCCAGCAAAACTGGGATTC
ATTCTTCCCAGCGTGATCTTGATTCTGCTTCAGGGCCCCAGGTATCCAACTTTACCCAGACGGT
AGACGCTCCTAATAGCATGGGACTGGAGCAGAACAAGGCTTTATCCTCAGCTGTGCAAGCCAG
CCCCACCTCTCCTGGGGGTTCTCCATCCTCTCCATCTTCTGGACAGCGGTCAGCAAGCCCTTC
AGTGCCGGGTCCCACTAAACCCAAACCAAAAACCAAACGGTTTCAGCTGCCTCTAGACAAAGG
GAATGGCAAGAAGCACAATGTTTCCCATTTGCGGACCAGTTCTTCTGAAGCACACATTCCAGA
CCAAGAAACGACATCCCTGACCTCAGGCACAGGGACTCCAGGAGCAGAGGCTGAGCAGCAG
GATACAGCTAGCGTGGAGCAGTCCTCCCAGAAGGAGTGTGGGCAACCTGCAGGGCAAGTCGC
TGTTCTTCCGGAAGTTCAGGTGACCCAAAATCCAGCAAATGAACAAGAAAGTGCAGAACCTAA
AACAGTGGAAGAAGAGGAAAGTAATTTCAGCTCCCCACTGATGCTTTGGCTTCAGCAAGAACA
AAAGCGGAAGGAAAGCATTACTGAGAAAAAACCCAAGAAAGGACTTGTTTTTGAAATTTCCAGT
GATGATGGCTTTCAGATCTGTGCAGAAAGTATTGAAGATGCCTGGAAGTCATTGACAGATAAAG
TCCAGGAAGCTCGATCAAATGCCCGCCTAAAGCAGCTCTCATTTGCAGGTGTTAACGGTTTGA
GGATGCTGGGGATTCTCCATGATGCAGTTGTGTTCCTCATTGAGCAGCTGTCTGGTGCCAAGC
ACTGTCGAAATTACAAATTCCGTTTCCACAAGCCAGAGGAGGCCAATGAACCCCCCTTGAACC
CTCACGGCTCAGCCAGGGCTGAAGTCCACCTCAGGAAGTCAGCATTTGACATGTTTAACTTCC
TGGCTTCTAAACATCGTCAGCCTCCTGAATACAACCCCAATGATGAAGAAGAGGAGGAGGTAC
AGCTGAAGTCAGCTCGGAGGGCAACTAGCATGGATCTGCCAATGCCCATGCGCTTCCGGCAC
TTAAAAAAGACTTCTAAGGAGGCAGTTGGTGTCTACAGGTCTCCCATCCATGGCCGGGGTCTT
TTCTGTAAGAGAAACATTGATGCAGGTGAGATGGTGATTGAGTATGCCGGCAACGTCATCCGC
TCCATCCAGACTGACAAGCGGGAAAAGTATTACGACAGCAAGGGCATTGGTTGCTATATGTTC
CGAATTGATGACTCAGAGGTAGTGGATGCCACCATGCATGGAAATGCTGCACGCTTCATCAAT
CACTCGTGTGAGCCTAACTGCTATTCTCGGGTCATCAATATTGATGGGCAGAAGCACATTGTCA
TCTTTGCCATGCGTAAGATCTACCGAGGAGAGGAACTCACTTACGACTATAAGTTCCCCATTGA
GGATGCCAGCAACAAGCTGCCCTGCAACTGTGGCGCTAAGAAATGCCGGAAGTTCCTAAACTA
A

B

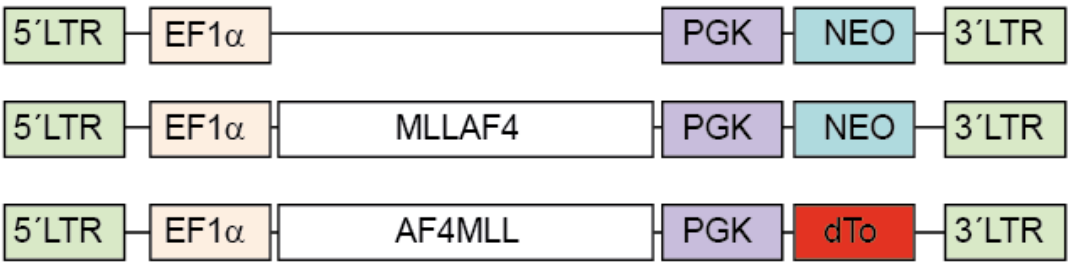
5´LTR
EF1α
PGK
NEO
3´LTR
5´LTR
EF1α
MLLAF4
PGK
NEO
3´LTR
5´LTR
EF1α
AF4MLL
PGK
dTo
3´LTR

A

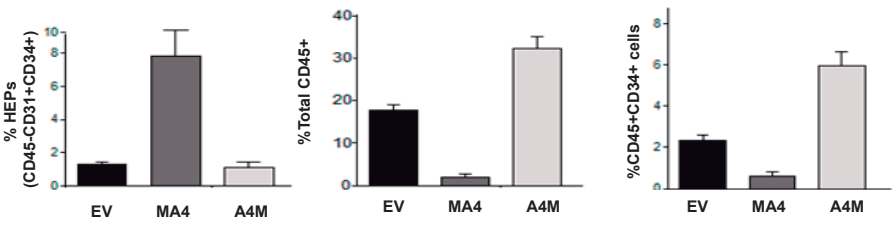
% HEPs (CD45-CD31+CD34+)
EV
MA4
A4M
% Total CD45+
EV
MA4
A4M
%CD45+CD34+ cells
EV
MA4
A4M

B

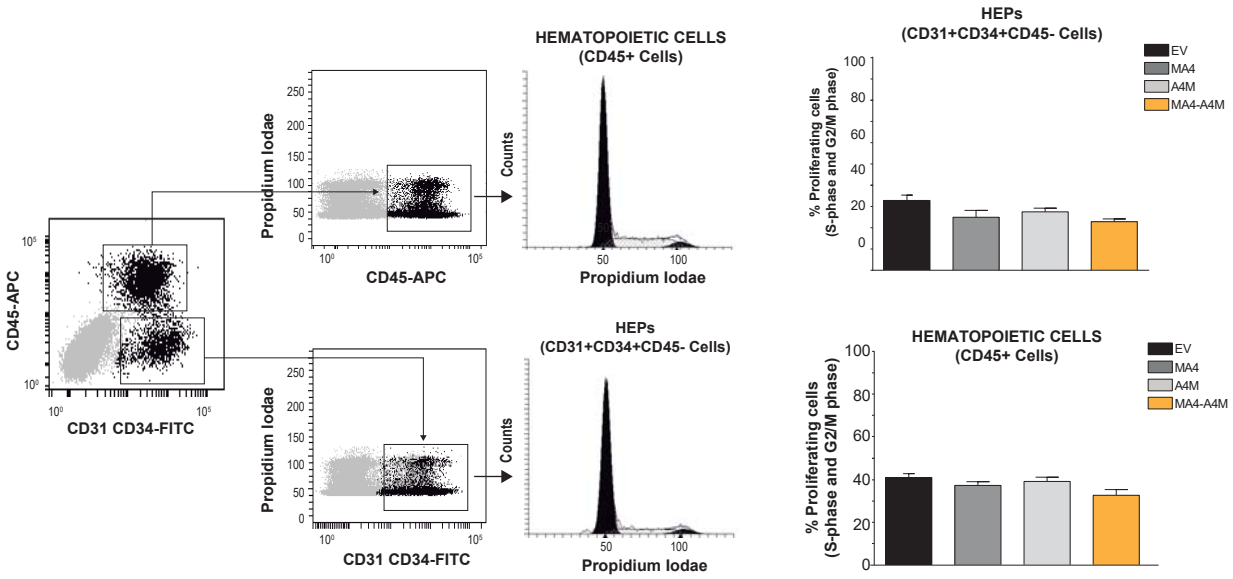
HEMATOPOIETIC CELLS (CD45+ Cells)
CD45-APC
CD31 CD34-FITC
Propidium Iodae
CD45-APC
Counts
Propidium Iodae
HEPs (CD31+CD34+CD45- Cells)
CD31 CD34-FITC
Propidium Iodae
HEPs (CD31+CD34+CD45- Cells)
% Proliferating cells (S-phase and G2/M phase)
EV
MA4
A4M
MA4-A4M
HEMATOPOIETIC CELLS (CD45+ Cells)
% Proliferating cells (S-phase and G2/M phase)
EV
MA4
A4M
MA4-A4M

C

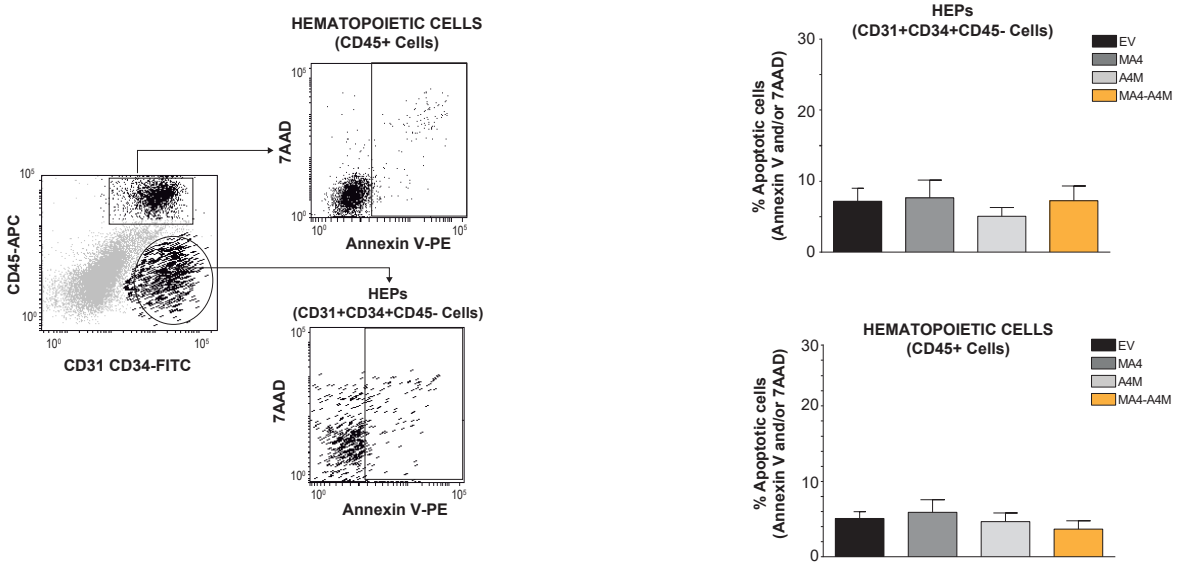
HEMATOPOIETIC CELLS (CD45+ Cells)
CD45-APC
CD31 CD34-FITC
7AAD
Annexin V-PE
HEPs (CD31+CD34+CD45- Cells)
7AAD
Annexin V-PE
HEPs (CD31+CD34+CD45- Cells)
% Apoptotic cells (Annexin V and/or 7AAD)
EV
MA4
A4M
MA4-A4M
HEMATOPOIETIC CELLS (CD45+ Cells)
% Apoptotic cells (Annexin V and/or 7AAD)
EV
MA4
A4M
MA4-A4M

A

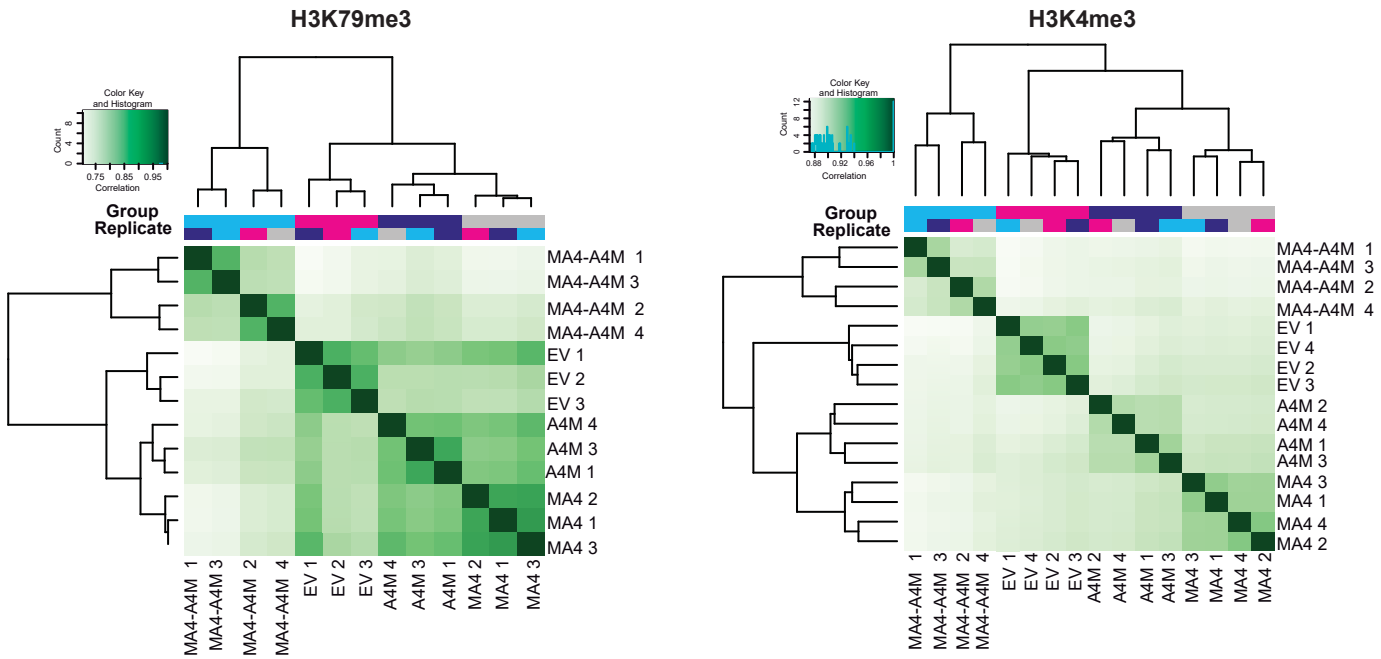
H3K79me3
Color Key and Histogram
Count
Correlation
Group
Replicate
MA4-A4M 1
MA4-A4M 3
MA4-A4M 2
MA4-A4M 4
EV 1
EV 2
EV 3
A4M 4
A4M 3
A4M 1
MA4 2
MA4 1
MA4 3
H3K4me3
Color Key and Histogram
Count
Correlation
Group
Replicate
MA4-A4M 1
MA4-A4M 3
MA4-A4M 2
MA4-A4M 4
EV 1
EV 4
EV 2
EV 3
A4M 2
A4M 4
A4M 1
A4M 3
MA4 3
MA4 1
MA4 4
MA4 2

B

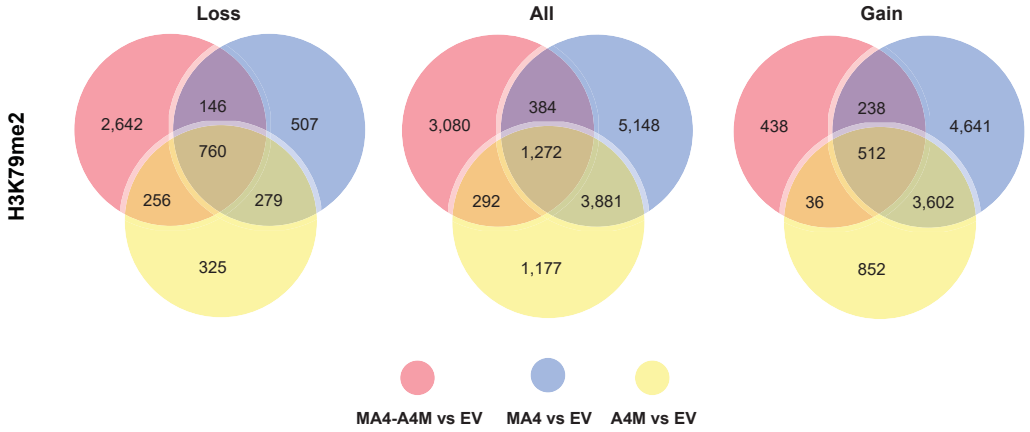
H3K79me2
Loss
2,642
146
507
760
256
279
325
All
3,080
384
5,148
1,272
292
3,881
1,177
Gain
438
238
4,641
512
36
3,602
852
MA4-A4M vs EV
MA4 vs EV
A4M vs EV

C

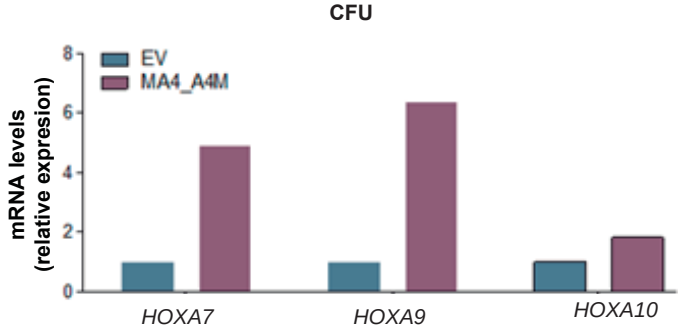
CFU
EV
MA4_A4M
mRNA levels
(relative expresion)
0
2
4
6
8
HOXA7
HOXA9
HOXA10

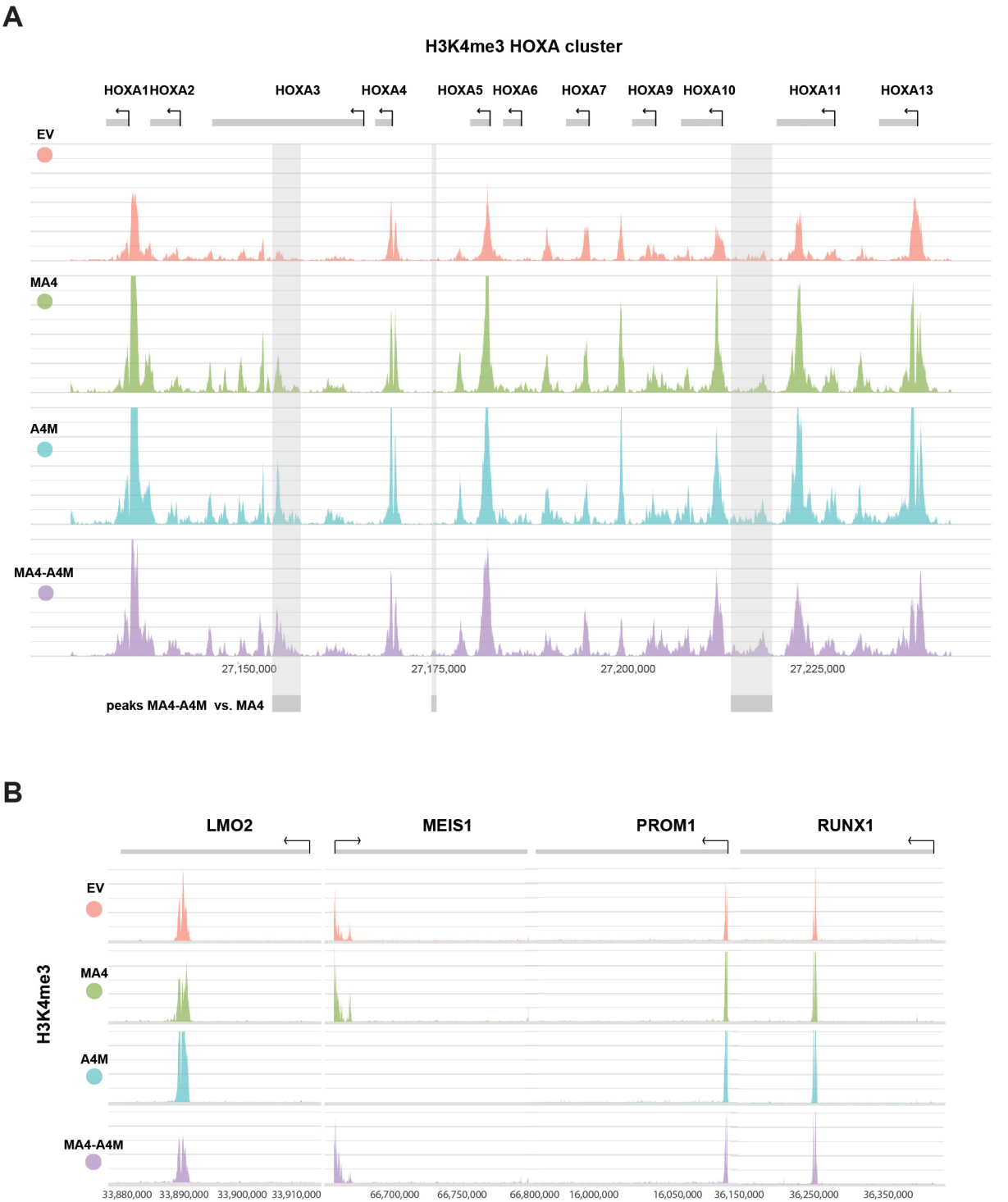
A
H3K4me3 HOXA cluster
HOXA1
HOXA2
HOXA3
HOXA4
HOXA5
HOXA6
HOXA7
HOXA9
HOXA10
HOXA11
HOXA13
EV
MA4
A4M
MA4-A4M
27,150,000
27,175,000
27,200,000
27,225,000
peaks MA4-A4M vs. MA4
B
LMO2
MEIS1
PROM1
RUNX1
H3K4me3
EV
MA4
A4M
MA4-A4M
33,880,000
33,890,000
33,900,000
33,910,000
66,700,000
66,750,000
66,800,000
16,000,000
16,050,000
36,150,000
36,250,000
36,350,000

SUPPLEMENTARY LEGENDS AND METHODS

Chromatin immunoprecipitation Sequencing

One million day 15 hematopoietic differentiating hEB-derived cells were subjected to Chromatin Immunoprecipitation (ChIP) as described [1]. Briefly, formaldehyde crosslinked cell extracts were sonicated using a Bioruptor (Diagenode) with a 0.5-min interval protocol to obtain DNA fragments of 200–500 bp. The chromatin fraction was divided into three parts and incubated overnight with 2 μg of anti-H3K4me3, anti-H3K79me3, or anti-H3 antibodies (Abcam) in RIPA buffer, and precipitated with protein A/G-Sepharose (Amersham). Cross-linkage of the co-precipitated DNA-protein complexes was reversed, and the DNA was sequenced at the CRG-CNAG Genomics Facility. Paired-end 50 bp ChIP-seq data reads were generated using a HiSeq 2500 Illumina sequencer. Alignment and peak detection was performed using the ENCODE (phase-3) histone ChIP-seq pipeline specifications. Reads were aligned to the human reference genome (assembly hg19) using BWA[2], removing all reads with a quality score <30. Peaks were called using MACS2[3] and whole cell extract samples as background samples. Differential analysis of histone mark peaks between experimental groups and the EV control group was performed using DiffBind[4], with a False Discovery Rate (FDR) cut-off of 0.1. Peaks annotation and Gene Ontology (GO) enrichment were analyzed with ChIP-Enrich package in R[4], using an FDR threshold of 0.1. ChIP-Seq data is deposited and available at Gene Expression Omnibus (GEO, accession number GSE111263).

Low-input RNA-seq and bulk RNA-seq on t(4;11)+B-ALL patients

For low-input RNAseq, 50 HEPs were FACS-purified from day 15 EBs into individual wells of a 96-well PCR plate containing lysis buffer (0.2% Triton-X100 and 2.3 U of SUPERase-In RNase Inhibitor; Ambion). Three independent replicates (50 cells/replicate) per condition were analyzed. RNA/cDNA was obtained and amplified as per the SMARTSEQ2 protocol[5,6]. Libraries were prepared for

sequencing using the Illumina Nextera XT DNA preparation kit. RNA-seq data was generated using a 50 single-end sequencing protocol. Pooled libraries were sequenced on the Illumina HiSeq 4000 platform. Reads were mapped to the human genome (Ensembl 81) and the ERCC sequences using STAR (version 2.4.2a) with default parameters. HTseq-count[7] was used to count the number of reads mapped to each gene with -s no (non-strand specific mode). Data were normalized for sequencing depth using the size factor from the DESeq2 package (version 1.12.2)[8]. Low-input RNA-seq data is deposited and available at GEO (GSE118947).

Bulk RNA-seq data on t(4;11)+ B-ALL patients was generated on the Illumina HiSeq 2500 platform using a 76 paired-end sequencing protocol and aligned to the human reference genome (hg19) using Tophat[19]. A gene was considered differentially expressed in MA4-A4M+ HEPs when it was >2-fold regulated ($p<0.01$) compared with the equivalent gene in EV-HEPs. Analysis of functional categories and biofunctions was performed with the genes differentially expressed using Ingenuity Pathway Analysis software (Ingenuity Inc., Redwood City, CA). Potential read pairs supporting the expression of MA4 and A4M fusion transcripts in patient samples were identified manually and with in-house written scripts as pairs in which each read aligned unambiguously to a different gene and which were compatible with the genomic breakpoints that were determined at the DNA level in all the samples. Additionally, RT-PCR with primers corresponding to *AF4* exon3 and *MLL* exon 12 (exons contained in all predicted fusions) was performed in all the samples to confirm the expression of any potential isoform of the reciprocal fusion gene. The identity of the isoform was confirmed by capillary sequencing. Finally, the expression of each fusion gene was determined by qRT-PCR using primer pairs spanning the breakpoint between genes. RNA-seq data is deposited and available at GEO (accession number GSE111263).

SUPPLEMENTARY REFERENCES

1. Guiu J, Bergen DJ, De Pater E, et al. Identification of Cdca7 as a novel Notch transcriptional target involved in hematopoietic stem cell emergence. *J Exp Med*. 2014;211(12):2411-2423.

2. Li H, Durbin R. Fast and accurate short read alignment with Burrows-Wheeler transform. *Bioinformatics*. 2009;25(14):1754-1760.

3. Zhang Y, Liu T, Meyer CA, et al. Model-based analysis of ChIP-Seq (MACS). *Genome Biol*. 2008;9(9):R137.

4. Welch RP, Lee C, Imbriano PM, et al. ChIP-Enrich: gene set enrichment testing for ChIP-seq data. *Nucleic Acids Res*. 2014;42(13):e105.

5. Picelli S, Bjorklund AK, Faridani OR, Sagasser S, Winberg G, Sandberg R. Smart-seq2 for sensitive full-length transcriptome profiling in single cells. *Nat Methods*. 2013;10(11):1096-1098.

6. Picelli S, Faridani OR, Bjorklund AK, Winberg G, Sagasser S, Sandberg R. Full-length RNA-seq from single cells using Smart-seq2. *Nat Protoc*. 2014;9(1):171-181.

7. Anders S, Pyl PT, Huber W. HTSeq--a Python framework to work with high-throughput sequencing data. *Bioinformatics*. 2015;31(2):166-169.

8. Love MI, Huber W, Anders S. Moderated estimation of fold change and dispersion for RNA-seq data with DESeq2. *Genome Biol*. 2014;15(12):550.

SUPPLEMENTARY LEGENDS

Figure S1. Coding sequence of the A4M fusion used in this study. (A) The full-length cDNA was sequenced-verified. Fusion breakpoint is located in AF4 exon 2 and MLL exon 10. (**B**) Schematic of lentivectors used in this study.

Figure S2. Co-expression of MA4 and A4M promotes specification rather than survival/proliferation of HEPs. (**A**) Day 20 MA4-expressing hEBs display a significant higher HEP production coupled to an impaired blood (CD45+ and CD45+CD34+) formation. (**B**) *Left*, representative FACS analysis of the identification of HEPs and $CD45^+$ hematopoietic cells and their cell-cycle distribution. *Right*, frequency of proliferating ($S+G_2M$ phases) CD45+ blood cells and HEPs. (**C**) *Left*, representative FACS analysis of apoptotic $CD45^+$ hematopoietic cells and HEPs. *Right*, frequency of apoptotic (Annexin V+) HEPs and CD45+ hematopoietic cells for the indicated genotypes.

Figure S3. H3K79me3 ChIP-seq profiles for the different genotypes. (**A**) Correlation heatmap for both H3K79me3 and H3K4me3 using affinity scores based on read counts in consensus peaks distinguishes between the four experimental groups. (**B**) Venn diagrams depicting the number of differentially enriched genomic regions for H3K79me3 between experimental groups relative to EV. (**C**) Quantitative expression of the indicated *HOX-A* genes in CFUs from day 15 EV- and double-fusion-expressing HEPs.

Figure S4. H3K4me2 profiles at genomic loci of MLL targets identified by Guenther *et al*. Representative profiles for ChIP-seq using an anti-$H3K4me^3$ antibody at genomic sites of HOX-A (**A**) and non-HOX (**B**) MLL targets in the indicated genotypes of human ESC-differentiating derivatives.

Table S1: Primers used in this study for RT-PCR.

GAPDH FW	GCACCGTCAAGGCTGAGAAC
GAPDH RV	AGGGATCTCGCTCCTGGAA
OCT4 FW	GGGTTTTTGGGATTAAGTTCTTCA
OCT4 RV	GCCCCCACCCTTTGTGTT
NANOG FW	ACAACTGGCCGAAGAATAGCA
NANOG RV	GGTTCCCAGTCGGGTTCAC
SOX2 FW	CAAAAATGGCCATGCAGGTT
SOX2 RV	AGTTGGGATCGAACAAAAGCTATT
DNMT3B FW	GCTCACAGGGCCCGATACTT
DNMT3B RV	GCAGTCCTGCAGCTCGAGTTTA
CRIPTO FW	CGGAACTGTGAGCACGATGT
CRIPTO RV	GGGCAGCCAGGTGTCATG
MLL-AF4 Fw	CAGGTCCAGAGCAGAGCAAAC
MLL-AF4 Rv	GAGCACTTGGAGGTGCAGATG
AF4-MLL Fw	GTTGCAATGCAGCAGAAGCC
AF4-MLL Rw	CAGGGTGATAGCTGTTTCGG

Table S2: Genes differentially expressed in double fusion-expressing as compared to control (EV) l

	geneID	baseMean	log2FoldChange	lfcSE	stat
ENSG00000112319	EYA4	119,7812612	-7,044862129	0,498747	-14,1251
ENSG00000197956	S100A6	74,70274938	-4,207670299	0,362337	-11,6126
ENSG00000159176	CSRP1	189,5093971	-4,448754354	0,433169	-10,2703
ENSG00000171735	CAMTA1	620,0966312	-2,63097972	0,26318	-9,99688
ENSG00000129595	EPB41L4A	143,8337732	-3,620551338	0,367992	-9,83866
ENSG00000121691	CAT	36,73876494	-4,619144396	0,469468	-9,83911
ENSG00000166770	ZNF667-AS1	26,47276123	-4,671600613	0,476384	-9,80638
ENSG00000053438	NNAT	16,76487505	-3,757812712	0,456726	-8,22772
ENSG00000166575	TMEM135	450,180446	-3,324034043	0,415462	-8,00081
ENSG00000257870	RP11-616L12.1	21,50131485	-4,406254358	0,581565	-7,57654
ENSG00000214872	SMTNL1	29,19194545	-4,020118702	0,547389	-7,34417
ENSG00000126947	ARMCX1	19,10444916	-3,661220371	0,518724	-7,05813
ENSG00000251379	RP11-484O2.1	11,01878906	-4,051707545	0,578618	-7,00239
ENSG00000158716	DUSP23	23,54803256	-3,475578813	0,520465	-6,67784
ENSG00000100644	HIF1A	792,004365	-2,324741527	0,349887	-6,64426
ENSG00000122966	CIT	309,5111002	-2,978040214	0,467302	-6,37283
ENSG00000145681	HAPLN1	1168,660196	-2,488794725	0,394148	-6,31436
ENSG00000123307	NEUROD4	14,76503349	-3,711665311	0,603199	-6,1533
ENSG00000151962	RBM46	8,6172188	-3,652100592	0,593965	-6,14868
ENSG00000164619	BMPER	82,57948722	-3,051493964	0,497697	-6,13122
ENSG00000100290	BIK	43,70310088	-3,317822269	0,541896	-6,12261
ENSG00000050555	LAMC3	20,06173885	-3,21721061	0,531609	-6,05184
ENSG00000167555	ZNF528	15,96797568	-3,401966116	0,57936	-5,87194
ENSG00000149179	C11orf49	373,9107859	-2,410856438	0,411459	-5,85929
ENSG00000137871	ZNF280D	37,3536919	-2,381859852	0,415608	-5,73103
ENSG00000165118	C9orf64	8,084483374	-3,283794749	0,596166	-5,50819
ENSG00000162654	GBP4	82,52014498	-2,47923141	0,458077	-5,41226
ENSG00000076716	GPC4	7,134763765	-3,24223284	0,608348	-5,32957
ENSG00000171476	HOPX	162,0285124	-2,521224355	0,474735	-5,3108
ENSG00000245680	ZNF585B	6,288623057	-3,047314734	0,578532	-5,26732
ENSG00000249252	RP11-665G4.1	10,94518525	-2,963291554	0,582687	-5,08556
ENSG00000142748	FCN3	240,9954012	-2,670085804	0,531573	-5,02299
ENSG00000143614	GATAD2B	90,16811689	-2,123176462	0,42897	-4,94947
ENSG00000185507	IRF7	11,90717047	-2,442768243	0,493898	-4,9459
ENSG00000134817	APLNR	237,009581	-2,180931226	0,442427	-4,92947
ENSG00000125170	DOK4	69,15447671	-1,872722463	0,380282	-4,92456
ENSG00000138315	OIT3	123,6956759	-2,82171733	0,579118	-4,87244
ENSG00000125775	SDCBP2	9,950851737	-2,868043853	0,589784	-4,86288
ENSG00000126709	IFI6	157,1396901	-2,135200905	0,44302	-4,81965
ENSG00000137942	FNBP1L	238,2318442	-1,143914856	0,240099	-4,76435
ENSG00000176728	TTTY14	7,465857067	-2,871826685	0,606999	-4,73119
ENSG00000118515	SGK1	94,59572992	-2,551626347	0,541541	-4,71178
ENSG00000108798	ABI3	32,92496542	-2,143701535	0,456145	-4,6996
ENSG00000008283	CYB561	12,17136654	-2,271524984	0,486907	-4,66522
ENSG00000188778	ADRB3	8,60506653	-2,566915557	0,554624	-4,62821
ENSG00000266472	MRPS21	256,7992655	-1,032266153	0,224316	-4,60184
ENSG00000253929	CASC21	10,99630532	-2,865101044	0,622643	-4,60151
ENSG00000113790	EHHADH	6,601260431	-2,771625162	0,620618	-4,46591
ENSG00000225792	AC004540.4	33,51932827	-2,490684309	0,564859	-4,40939
ENSG00000253438	PCAT1	26,94528599	-2,547965544	0,579052	-4,40024
ENSG00000095015	MAP3K1	44,49573983	-1,601596875	0,366684	-4,36778
ENSG00000280079	CTC-260E6.4	4,201191271	-2,612039681	0,613045	-4,26077
ENSG00000089050	RBBP9	18,85931665	-2,239301793	0,528577	-4,23647

Downregulated

ENSG00000109501	WFS1	11,45922699	-2,297305349	0,545604	-4,21057
ENSG00000105750	ZNF85	35,18030151	-2,03086483	0,485118	-4,18633
ENSG00000188643	S100A16	658,5606704	-1,602025271	0,386902	-4,14065
ENSG00000050628	PTGER3	22,15704024	-2,396796376	0,57973	-4,13433
ENSG00000113209	PCDHB5	4,603009559	-2,561413963	0,622412	-4,1153
ENSG00000169255	B3GALNT1	6,456259068	-2,420174153	0,5913	-4,09297
ENSG00000138835	RGS3	134,7621143	-1,343148381	0,328301	-4,09121
ENSG00000115461	IGFBP5	43,88760757	-2,456376257	0,607117	-4,04597
ENSG00000167941	SOST	55,5937508	-2,329603289	0,582511	-3,99924
ENSG00000128602	SMO	4,201100881	-2,331501814	0,589037	-3,95816
ENSG00000184220	CMSS1	99,07782163	-1,184435761	0,299615	-3,95319
ENSG00000196814	MVB12B	18,6907974	-2,36958793	0,600272	-3,94753
ENSG00000165259	HDX	3,752930822	-2,416387304	0,615296	-3,92719
ENSG00000137216	TMEM63B	40,97473872	-2,191833358	0,557964	-3,92827
ENSG00000166482	MFAP4	33,74531096	-2,36800861	0,604369	-3,91815
ENSG00000100888	CHD8	120,5148935	-1,370548703	0,35098	-3,90492
ENSG00000198785	GRIN3A	5,057809271	-2,433961659	0,624515	-3,89736
ENSG00000128040	SPINK2	17,31695007	-2,409310609	0,62118	-3,8786
ENSG00000184344	GDF3	47,03429759	-1,608254011	0,414806	-3,87713
ENSG00000172269	DPAGT1	91,17134944	-0,973958418	0,252828	-3,85225
ENSG00000103978	TMEM87A	77,09366437	-0,930827779	0,242655	-3,83602
ENSG00000197859	ADAMTSL2	3,993914273	-2,377353556	0,6191	-3,84001
ENSG00000157152	SYN2	9,446479206	-2,307034408	0,601271	-3,83693
ENSG00000180543	TSPYL5	3,622665339	-2,329868038	0,609108	-3,82505
ENSG00000132622	HSPA12B	7,527287149	-2,359294514	0,618173	-3,81656
ENSG00000154783	FGD5	64,4228883	-1,548935262	0,406995	-3,80578
ENSG00000221923	ZNF880	9,214690052	-2,304807456	0,609095	-3,78399
ENSG00000267383	CTC-260E6.6	3,883965663	-2,232586548	0,592887	-3,76562
ENSG00000120708	TGFBI	91,70684239	-2,076734506	0,551285	-3,76708
ENSG00000278318	ZNF229	6,000326955	-2,312454347	0,614696	-3,76195
ENSG00000182853	VMO1	5,507887137	-2,345260449	0,625084	-3,75191
ENSG00000109099	PMP22	191,524615	-1,714779803	0,458	-3,74406
ENSG00000143621	ILF2	779,2962781	-0,763125525	0,20397	-3,74137
ENSG00000156535	CD109	92,89720586	-1,532077411	0,413633	-3,70395
ENSG00000164053	ATRIP	11,14423421	-1,996586023	0,539181	-3,703
ENSG00000269834	ZNF528-AS1	5,822155471	-2,246975187	0,607714	-3,69742
ENSG00000136869	TLR4	36,50193073	-1,968054924	0,534075	-3,68498
ENSG00000133636	NTS	263,7477271	-1,851710654	0,505231	-3,66508
ENSG00000183072	NKX2-5	7,504153845	-2,287599283	0,624984	-3,66025
ENSG00000171227	TMEM37	64,20801532	-1,828344024	0,501254	-3,64754
ENSG00000118523	CTGF	23,79760678	-2,05484338	0,564356	-3,64104
ENSG00000143878	RHOB	123,0762709	-1,165082318	0,320141	-3,63927
ENSG00000228065	LINC01515	9,063863586	-2,161801995	0,594472	-3,6365
ENSG00000105825	TFPI2	148,9275203	-2,004539393	0,555907	-3,60589
ENSG00000198046	ZNF667	4,673953372	-2,203789836	0,612935	-3,59547
ENSG00000128463	EMC4	243,526124	-1,020257843	0,284652	-3,58422
ENSG00000129219	PLD2	20,75205268	-1,844978284	0,515983	-3,57566
ENSG00000198155	ZNF876P	21,53321141	-1,858631803	0,520801	-3,56879
ENSG00000154864	PIEZO2	10,72154092	-2,04403594	0,574046	-3,56075
ENSG00000188167	TMPPE	8,499811893	-2,171684721	0,610707	-3,55602
ENSG00000167085	PHB	160,4917939	-0,728482562	0,206203	-3,53284
ENSG00000079308	TNS1	15,59828255	-1,907912201	0,542247	-3,51853
ENSG00000173068	BNC2	7,553218219	-2,072085911	0,589584	-3,51449
ENSG00000140937	CDH11	38,05932655	-1,818437228	0,517773	-3,51203
ENSG00000214022	REPIN1	16,34937523	-1,45512511	0,4145	-3,51055

ENSG00000145623	OSMR	22,88032432	-1,714715805	0,48917	-3,50536
ENSG00000134107	BHLHE40	29,32775574	-1,724282256	0,49275	-3,49931
ENSG00000137959	IFI44L	24,12130347	-2,143875186	0,618601	-3,46569
ENSG00000075336	TIMM21	62,0256047	-1,334155081	0,387092	-3,44661
ENSG00000075213	SEMA3A	4,414059558	-2,148672606	0,624614	-3,44
ENSG00000123411	IKZF4	5,955377563	-2,037072187	0,594437	-3,42689
ENSG00000187123	LYPD6	11,07461616	-2,026908881	0,593353	-3,41602
ENSG00000101955	SRPX	28,49768115	-1,900070277	0,559264	-3,39745
ENSG00000132718	SYT11	7,459581183	-2,085624327	0,614559	-3,39369
ENSG00000116871	MAP7D1	63,43010166	-1,164518143	0,344658	-3,37876
ENSG00000221914	PPP2R2A	127,74934	-1,213673571	0,359423	-3,37673
ENSG00000136111	TBC1D4	91,02589998	-1,505884231	0,447621	-3,3642
ENSG00000260589	STAM-AS1	6,353032422	-2,061083344	0,613598	-3,35901
ENSG00000104883	PEX11G	3,473941597	-2,041500351	0,608034	-3,35755
ENSG00000128656	CHN1	22,22951211	-1,754175298	0,524292	-3,3458
ENSG00000100804	PSMB5	1009,211466	-0,468827604	0,140839	-3,32882
ENSG00000143387	CTSK	20,76828404	-1,906330014	0,573337	-3,32497
ENSG00000161298	ZNF382	15,38563794	-1,959869444	0,590249	-3,32041
ENSG00000197879	MYO1C	52,84678543	-1,454858668	0,43873	-3,31607
ENSG00000088756	ARHGAP28	115,6586262	-1,596855186	0,481915	-3,31356
ENSG00000023734	STRAP	462,0612498	-0,747464329	0,22603	-3,30693
ENSG00000165507	C10orf10	220,6959202	-1,658443129	0,50289	-3,29782
ENSG00000075043	KCNQ2	6,601271751	-2,061423654	0,624991	-3,29832
ENSG00000112414	ADGRG6	36,47477989	-1,745878365	0,529655	-3,29626
ENSG00000077616	NAALAD2	56,93366239	-1,520442973	0,462829	-3,28511
ENSG00000075914	EXOSC7	194,602295	-0,783595705	0,239541	-3,27124
ENSG00000171206	TRIM8	63,84318428	-0,865536936	0,264592	-3,27121
ENSG00000118257	NRP2	283,4681789	-1,532317765	0,469263	-3,26537
ENSG00000143127	ITGA10	10,03941541	-1,785434325	0,547072	-3,26362
ENSG00000023697	DERA	150,4101781	-0,681082172	0,208571	-3,26547
ENSG00000118777	ABCG2	3,843971196	-2,022242023	0,623639	-3,24265
ENSG00000187608	ISG15	184,3901201	-1,394462458	0,429952	-3,24329
ENSG00000126458	RRAS	57,58634609	-1,451973482	0,448239	-3,23928
ENSG00000165449	SLC16A9	16,46524127	-1,890504921	0,585565	-3,22851
ENSG00000184602	SNN	32,10538075	-1,634277643	0,507691	-3,21904
ENSG00000127241	MASP1	23,24454565	-1,845003945	0,576404	-3,20089
ENSG00000149948	HMGA2	90,72469841	-1,52121514	0,475166	-3,20144
ENSG00000114021	NIT2	84,62290275	-1,153181957	0,360509	-3,19876
ENSG00000184384	MAML2	14,57290268	-1,826824148	0,572071	-3,19335
ENSG00000242616	GNG10	6,482908148	-1,554933346	0,488834	-3,1809
ENSG00000148677	ANKRD1	4,28010366	-1,970424552	0,622291	-3,1664
ENSG00000196549	MME	3,945823194	-1,974427338	0,625005	-3,15906
ENSG00000253983	RP1-16A9.1	14,33422465	-1,874651488	0,594221	-3,15481
ENSG00000148516	ZEB1	70,75457064	-1,201599666	0,380806	-3,15541
ENSG00000005448	WDR54	242,8808433	-0,998035849	0,316873	-3,14964
ENSG00000154174	TOMM70A	68,10833425	-1,029143057	0,326615	-3,15094
ENSG00000132256	TRIM5	97,54230397	-1,156660563	0,368004	-3,14307
ENSG00000101230	ISM1	3,50609647	-1,959429369	0,624987	-3,13515
ENSG00000237187	NR2F1-AS1	2,905463012	-1,955399501	0,624047	-3,13342
ENSG00000242193	RP11-568K15.1	3,073799555	-1,950988371	0,623719	-3,12799
ENSG00000130299	GTPBP3	13,910181	-1,466872176	0,471831	-3,1089
ENSG00000154451	GBP5	9,678934476	-1,802622749	0,579799	-3,10905
ENSG00000142065	ZFP14	15,70823406	-1,538362857	0,495279	-3,10605
ENSG00000108352	RAPGEFL1	5,309428532	-1,91989045	0,623119	-3,0811
ENSG00000196611	MMP1	14,43198215	-1,892234278	0,614911	-3,07725

Downregulated

ENSG00000136546	SCN7A	7,310132654	-1,9043461	0,619072	-3,07613
ENSG00000182983	ZNF662	5,485208999	-1,918878485	0,624159	-3,07434
ENSG00000155438	NIFK	129,0123703	-0,987586753	0,321598	-3,07088
ENSG00000254615	RP11-395G23.3	15,42007794	-1,887702828	0,614815	-3,07036
ENSG00000233056	ERVH48-1	27,2291599	-1,801462596	0,587193	-3,06792
ENSG00000074219	TEAD2	29,84254346	-1,248631404	0,408137	-3,05934
ENSG00000267152	CTD-2528L19.6	4,012936355	-1,884323661	0,617433	-3,05187
ENSG00000197479	PCDHB11	3,421521002	-1,894232329	0,621873	-3,04601
ENSG00000151746	BICD1	67,26482608	-0,959827076	0,314971	-3,04736
ENSG00000254202	RP11-120I21.2	4,008818691	-1,904714553	0,625006	-3,04751
ENSG00000100379	KCTD17	5,170316551	-1,851441418	0,608966	-3,0403
ENSG00000232282	MTND1P32	5,013687738	-1,787125704	0,588479	-3,03686

human ESC-derievd HEPs	
pvalue	**padj**
2,65937E-45	3,67046E-41
3,55721E-31	2,45483E-27
9,59483E-25	4,41426E-21
1,57275E-23	5,42676E-20
7,67258E-23	1,76495E-19
7,63836E-23	1,76495E-19
1,05687E-22	2,08385E-19
1,90803E-16	3,29182E-13
1,23598E-15	1,89545E-12
3,54881E-14	4,89806E-11
2,07039E-13	2,59778E-10
1,68761E-12	1,94103E-09
2,51638E-12	2,67162E-09
2,42493E-11	2,39064E-08
3,04737E-11	2,80399E-08
1,85566E-10	1,42288E-07
2,7128E-10	1,8721E-07
7,58848E-10	4,90169E-07
7,81315E-10	4,90169E-07
8,72064E-10	5,23314E-07
9,2052E-10	5,29376E-07
1,43205E-09	7,90605E-07
4,30731E-09	2,28652E-06
4,64862E-09	2,3763E-06
9,98235E-09	4,92059E-06
3,62548E-08	1,61416E-05
6,22348E-08	2,68426E-05
9,8446E-08	4,11743E-05
1,09144E-07	4,4306E-05
1,38431E-07	5,45892E-05
3,66539E-07	0,000136729
5,08737E-07	0,000184779
7,44147E-07	0,000253558
7,57945E-07	0,000253558
8,24518E-07	0,000264651
8,45503E-07	0,000265219
1,10229E-06	0,000338085
1,15693E-06	0,000347128
1,43812E-06	0,000422318
1,89459E-06	0,000533656
2,2321E-06	0,000616149
2,45557E-06	0,000651765
2,60668E-06	0,00067882
3,08292E-06	0,000787972
3,68849E-06	0,000925609
4,18767E-06	0,000998112
4,19436E-06	0,000998112
7,97286E-06	0,001774861
1,03662E-05	0,002167795
1,08133E-05	0,002227541
1,25515E-05	0,002547587
2,03728E-05	0,004016928
2,27059E-05	0,004352602

2,54723E-05	0,004750937
2,835E-05	0,005217147
3,46317E-05	0,00612804
3,55985E-05	0,006219366
3,8667E-05	0,00658866
4,25878E-05	0,007136073
4,29136E-05	0,007136073
5,21073E-05	0,008362615
6,35458E-05	0,009854603
7,55309E-05	0,011209432
7,71153E-05	0,01132282
7,89632E-05	0,011472109
8,59434E-05	0,012103985
8,55588E-05	0,012103985
8,92307E-05	0,012315615
9,42571E-05	0,012389866
9,72454E-05	0,012543749
0,000105058	0,013262173
0,000105698	0,013262173
0,000117036	0,014294925
0,000125044	0,014625965
0,000123027	0,014625965
0,000124583	0,014625965
0,000130746	0,015115894
0,000135327	0,015436191
0,000141356	0,015861789
0,000154337	0,01704122
0,000166139	0,017683711
0,000165167	0,017683711
0,000168596	0,017763055
0,000175491	0,018135494
0,000181069	0,018399483
0,000183022	0,018438446
0,000212265	0,020856574
0,000213069	0,020856574
0,000217801	0,021021558
0,000228719	0,021922119
0,000247264	0,02337491
0,000251965	0,02365728
0,000264761	0,024361506
0,000271537	0,024819604
0,000273408	0,02482613
0,000276363	0,024930441
0,000311083	0,027174458
0,000323803	0,027668608
0,000338083	0,028592402
0,000349346	0,028604101
0,000358631	0,028946321
0,000369797	0,029332995
0,000376517	0,029695374
0,000411117	0,031699643
0,00043395	0,033090453
0,0004406	0,033413007
0,00044469	0,033538835
0,000447178	0,033543185

0,000455997	0,03383694
0,000466469	0,034428918
0,000528881	0,03821791
0,000567671	0,04017947
0,000581708	0,040962946
0,000610534	0,042344668
0,000635429	0,04341682
0,000680172	0,045956658
0,00068957	0,046201173
0,000728129	0,04831556
0,000733541	0,048441817
0,000767663	0,050214628
0,000782222	0,050717732
0,000786378	0,050717732
0,000820459	0,051944817
0,000872143	0,054467501
0,000884268	0,05472946
0,000898844	0,055383247
0,000912935	0,055794581
0,000921155	0,055999562
0,000943249	0,056648967
0,000974369	0,05771778
0,000972638	0,05771778
0,000979817	0,05779244
0,001019422	0,059618936
0,001070774	0,061583923
0,00107087	0,061583923
0,001093206	0,062221032
0,001099981	0,062221032
0,001092818	0,062221032
0,001184252	0,065642763
0,001181559	0,065642763
0,001198307	0,06615611
0,001244357	0,068420139
0,001286198	0,070166444
0,001370054	0,073577751
0,00136742	0,073577751
0,001380191	0,073834882
0,001406304	0,074653128
0,001468168	0,076466642
0,00154336	0,07948306
0,001582788	0,080909803
0,001606039	0,081494681
0,001602702	0,081494681
0,001634742	0,081844726
0,001627458	0,081844726
0,001671879	0,08319453
0,001717651	0,083770398
0,001727833	0,083970246
0,00176006	0,085236321
0,001877877	0,089475562
0,001876901	0,089475562
0,001896032	0,089619958
0,002062386	0,094255126
0,002089211	0,095165992

0,002097054	0,095208998
0,002109675	0,095310888
0,002134309	0,095498626
0,002138029	0,095498626
0,002155533	0,095661302
0,002218229	0,096297492
0,002274211	0,097783968
0,002318974	0,098178394
0,002308647	0,098178394
0,002307441	0,098178394
0,002363398	0,0985487
0,002390582	0,099354233

Table S3:

Regions differentially enriched in H3K79me3 between double fusion- and MA4/EV-hESC blood derivative

peak_id	peak_start	peak_end	7E+05	locus_start	locus_end	gene_symb	overlap_star	overlap_end
peak:1	21618836	21619430	594	21554783	21719308	ECE1	21618836	21619430
peak:2	27871020	27871960	940	27767914	27873410	WASF2	27871020	27871960
peak:3	41155277	41157219	1942	41144284	41157806	NFYC	41155277	41157219
peak:4	43767794	43768815	1021	43758928	43795178	TIE1	43767794	43768815
peak:5	47695316	47696362	1046	47672771	47723818	TAL1	47695316	47696362
peak:6	52092228	52092904	676	52013924	52263685	OSBPL9	52092228	52092904
peak:7	62226710	62227754	1044	62199623	62549757	PATJ	62226710	62227754
peak:8	91852668	91853280	612	91650423	91918415	HFM1	91852668	91853280
peak:9	92280907	92281736	829	92153990	92393243	TGFBR3	92280907	92281736
peak:10	94703947	94704550	603	94624102	94812278	ARHGAP29	94703947	94704550
peak:11	108502605	108503363	758	108079204	108621488	VAV3	108502605	108503363
peak:12	114481375	114482734	1359	114459956	114514019	HIPK1	114481375	114482734
peak:13	120176292	120176979	687	120166153	120222404	ZNF697	120176292	120176979
peak:14	154463886	154464492	606	154426098	154474610	SHE	154463886	154464492
peak:15	157250423	157251400	977	157103269	157315346	ETV3	157250423	157251400
peak:16	157986113	157987159	1046	157887349	158103061	KIRREL	157986113	157987159
peak:17	163039109	163041536	2427	162938501	163107329	RGS4	163039109	163041536
peak:18	183783701	183785394	1693	183698362	183845013	RGL1	183783701	183785394
peak:19	201510376	201510995	619	201482710	201553241	RPS10P7	201510376	201510995
peak:20	204647245	204647779	534	204574483	204726189	LRRN2	204647245	204647779
peak:21	208383479	208384731	1252	208143618	209009916	PLXNA2	208383479	208384731
peak:22	220703366	220703980	614	220573706	220782598	MARK1	220703366	220703980
peak:23	232629101	232629915	814	232276214	232795940	SIPA1L2	232629101	232629915
peak:24	17932183	17934084	1901	17824513	17935136	SMC6	17932183	17934084
peak:25	28634051	28635122	1071	28417452	28668758	FOSL2	28634051	28635122
peak:26	46534835	46535854	1019	46214208	46656771	EPAS1	46534835	46535854
peak:27	48759327	48760668	1341	48712609	48801122	STON1	48759327	48760668
peak:28	54168333	54168855	522	54100888	54270193	PSME4	54168333	54168855
peak:29	54690992	54692859	1867	54620763	54720378	SPTBN1	54690992	54692859
peak:30	54702819	54703781	962	54620763	54720378	SPTBN1	54702819	54703781
peak:31	72644998	72645642	644	72099974	72714084	CYP26B1	72644998	72645642
peak:32	109229797	109230389	592	109108195	109303602	LIMS1	109229797	109230389
peak:33	109234180	109234886	706	109108195	109303602	LIMS1	109234180	109234886
peak:34	120125114	120125747	633	120124455	120157348	DBI	120125114	120125747
peak:35	121019287	121019855	568	120989313	121057066	RALB	121019287	121019855
peak:36	121029069	121029803	734	120989313	121057066	RALB	121029069	121029803
peak:37	128113068	128113860	792	128076279	128138400	MAP3K2	128113068	128113860
peak:38	133011780	133012292	512	132967090	133015097	MIR663B	133011780	133012292
peak:39	133038386	133038832	446	133015098	133094844	ANKRD30BL	133038386	133038832
peak:40	145187137	145187678	541	145182640	145351746	ZEB2	145187137	145187678
peak:41	145214821	145215668	847	145182640	145351746	ZEB2	145214821	145215668
peak:42	145235431	145235972	541	145182640	145351746	ZEB2	145235431	145235972
peak:43	149902014	149904254	2240	149875716	150060267	LYPD6B	149902014	149904254
peak:44	165598915	165600426	1511	165516586	165755356	COBLL1	165598915	165600426
peak:45	169333032	169334164	1132	169208433	169376106	CERS6	169333032	169334164
peak:46	169337729	169338323	594	169208433	169376106	CERS6	169337729	169338323
peak:47	175525268	175526385	1117	175407155	175588413	WIPF1	175525268	175526385

peak:48	175695012	175695857	845	175670774	175951272	CHN1	175695012	175695857
peak:49	175707639	175708499	860	175670774	175951272	CHN1	175707639	175708499
peak:50	177146909	177147362	453	177093905	177299951	MTX2	177146909	177147362
peak:51	188300740	188301564	824	188013460	188366120	CALCRL	188300740	188301564
peak:52	188303927	188304492	565	188013460	188366120	CALCRL	188303927	188304492
peak:53	188305395	188306865	1470	188013460	188366120	CALCRL	188305395	188306865
peak:54	188308114	188308817	703	188013460	188366120	CALCRL	188308114	188308817
peak:55	188311462	188312080	618	188013460	188366120	CALCRL	188311462	188312080
peak:56	188408262	188409936	1674	188366121	188787807	TFPI	188408262	188409936
peak:57	189838944	189842924	3980	189746966	189840958	COL3A1	189838944	189840958
peak:57	189838944	189842924	3980	189840959	189842852	MIR1245A	189840959	189842852
peak:57	189838944	189842924	3980	189842853	189849641	MIR1245B	189842853	189842924
peak:58	189844676	189851425	6749	189842853	189849641	MIR1245B	189844676	189849641
peak:58	189844676	189851425	6749	189849642	189858375	COL3A1	189849642	189851425
peak:59	190021826	190023085	1259	190021222	190175382	COL5A2	190021826	190023085
peak:60	204395160	204398532	3372	204329741	204485628	RAPH1	204395160	204398532
peak:61	218706287	218706682	395	218650028	218883687	TNS1	218706287	218706682
peak:62	218715866	218716708	842	218650028	218883687	TNS1	218715866	218716708
peak:63	218716730	218719036	2306	218650028	218883687	TNS1	218716730	218719036
peak:64	225815144	225815631	487	225560167	225843518	DOCK10	225815144	225815631
peak:65	238298545	238299318	773	238123121	238358951	COL6A3	238298545	238299318
peak:66	238300753	238301271	518	238123121	238358951	COL6A3	238300753	238301271
peak:67	238304977	238305456	479	238123121	238358951	COL6A3	238304977	238305456
peak:68	238306153	238309255	3102	238123121	238358951	COL6A3	238306153	238309255
peak:69	238621449	238621986	537	238517997	238692545	LRRFIP1	238621449	238621986
peak:70	240135369	240136093	724	240114464	240168743	MGC16025	240135369	240136093
peak:71	240145501	240146534	1033	240114464	240168743	MGC16025	240145501	240146534
peak:72	240149333	240149905	572	240114464	240168743	MGC16025	240149333	240149905
peak:73	240212422	240213123	701	240168744	240223745	HDAC4	240212422	240213123
peak:74	240228231	240229136	905	240223746	240250328	MIR4269	240228231	240229136
peak:75	8554114	8554720	606	8018481	8578480	LMCD1	8554114	8554720
peak:76	8554930	8556174	1244	8018481	8578480	LMCD1	8554930	8556174
peak:77	8556581	8557182	601	8018481	8578480	LMCD1	8556581	8557182
peak:78	8559899	8560829	930	8018481	8578480	LMCD1	8559899	8560829
peak:79	14763030	14763577	547	14708493	14829669	C3orf20	14763030	14763577
peak:80	14853968	14855571	1603	14829670	14956524	FGD5	14853968	14855571
peak:81	17917820	17918600	780	17162158	18125534	TBC1D5	17917820	17918600
peak:82	52085036	52085872	836	52060210	52094794	DUSP7	52085036	52085872
peak:83	55508987	55510075	1088	55238517	55583304	WNT5A	55508987	55510075
peak:84	56795772	56796406	634	56763366	57022484	ARHGEF3	56795772	56796406
peak:85	63842015	63843350	1335	63827320	63849915	THOC7	63842015	63843350
peak:86	69279329	69280973	1644	69210728	69690159	FRMD4B	69279329	69280973
peak:87	73591060	73591723	663	73296906	74122207	PDZRN3	73591060	73591723
peak:88	73599291	73601321	2030	73296906	74122207	PDZRN3	73599291	73601321
peak:89	73641145	73641964	819	73296906	74122207	PDZRN3	73641145	73641964
peak:90	73658671	73660460	1789	73296906	74122207	PDZRN3	73658671	73660460
peak:91	79061908	79062259	351	78178797	80804919	ROBO1	79061908	79062259
peak:92	93710720	93711323	603	93695959	93723218	ARL13B	93710720	93711323
peak:93	149258030	149258652	622	149143969	149283738	TM4SF4	149258030	149258652
peak:94	149301705	149302474	769	149283739	149445700	WWTR1	149301705	149302474

peak:95	149319672	149320175	503	149283739	149445700	WWTR1	149319672	149320175
peak:96	149322137	149323389	1252	149283739	149445700	WWTR1	149322137	149323389
peak:97	149341930	149343051	1121	149283739	149445700	WWTR1	149341930	149343051
peak:98	150464111	150464934	823	150451503	150570405	SIAH2	150464111	150464934
peak:99	150821094	150821835	741	150747119	150862786	MED12L	150821094	150821835
peak:100	152556204	152556776	572	152342734	152716382	P2RY1	152556204	152556776
peak:101	155618589	155619233	644	155580287	155713331	GMPS	155618589	155619233
peak:102	169878401	169879141	740	169827626	169919878	PHC3	169878401	169879141
peak:103	171518375	171518966	591	171285301	171544821	PLD1	171518375	171518966
peak:104	498352	498925	573	492975	556220	PIGG	498352	498925
peak:105	11411842	11412580	738	11400495	12458263	HS3ST1	11411842	11412580
peak:106	16849393	16850772	1379	16649796	17207140	LDB2	16849393	16850772
peak:107	16870346	16871132	786	16649796	17207140	LDB2	16870346	16871132
peak:108	41201940	41202563	623	40805544	41237766	APBB2	41201940	41202563
peak:109	41433689	41434541	852	41310852	41722979	LIMCH1	41433689	41434541
peak:110	46316153	46316998	845	46258740	46651836	GABRA2	46316153	46316998
peak:111	55968864	55970391	1527	55792673	56102075	KDR	55968864	55970391
peak:112	55976377	55977009	632	55792673	56102075	KDR	55976377	55977009
peak:113	56407226	56411318	4092	56288872	56435727	CLOCK	56407226	56411318
peak:114	70296489	70296866	377	70253922	70448546	UGT2B4	70296489	70296866
peak:115	89078604	89079070	466	89013107	89179228	ABCG2	89078604	89079070
peak:116	98336060	98336772	712	97912816	99123459	STPG2	98336060	98336772
peak:117	99503131	99503880	749	99380664	99715027	TSPAN5	99503131	99503880
peak:118	102236712	102237215	503	101932450	102268781	PPP3CA	102236712	102237215
peak:119	106819006	106819440	434	106724284	106992738	NPNT	106819006	106819440
peak:120	111560606	111561890	1284	111470742	112314916	PITX2	111560606	111561890
peak:121	111561918	111563250	1332	111470742	112314916	PITX2	111561918	111563250
peak:122	121989051	121990325	1274	121918844	122039584	NDNF	121989051	121990325
peak:123	140866867	140867382	515	140831078	141126836	MAML3	140866867	140867382
peak:124	170532926	170533631	705	170356299	170537725	NEK1	170532926	170533631
peak:125	171970641	171971262	621	171872974	173412239	GALNTL6	171970641	171971262
peak:126	174451585	174455688	4103	174389030	174828103	HAND2	174451585	174455688
peak:127	174456733	174457313	580	174389030	174828103	HAND2	174456733	174457313
peak:128	177700357	177701207	850	177477493	177972443	VEGFC	177700357	177701207
peak:129	33815995	33816342	347	33666504	33914307	ADAMTS12	33815995	33816342
peak:130	34682324	34683635	1311	34349903	34763466	RAI14	34682324	34683635
peak:131	71146585	71147075	490	70956662	71209054	CARTPT	71146585	71147075
peak:132	75915631	75916611	980	75912092	75944780	F2RL2	75915631	75916611
peak:133	75916941	75919331	2390	75912092	75944780	F2RL2	75916941	75919331
peak:134	76015283	76017317	2034	76010049	76063350	F2R	76015283	76017317
peak:135	82842228	82843032	804	82634807	82900423	VCAN	82842228	82843032
peak:136	82993967	82995862	1895	82900424	83195771	HAPLN1	82993967	82995862
peak:137	83675308	83675942	634	83195772	84629436	EDIL3	83675308	83675942
peak:138	88678070	88678649	579	88050183	88756229	MEF2C	88678070	88678649
peak:139	119438659	119439276	617	119382637	120570241	PRR16	119438659	119439276
peak:140	134371684	134378062	6378	134369468	134528599	PITX1	134371684	134378062
peak:141	134378989	134379580	591	134369468	134528599	PITX1	134378989	134379580
peak:142	134379602	134380282	680	134369468	134528599	PITX1	134379602	134380282
peak:143	134380973	134381561	588	134369468	134528599	PITX1	134380973	134381561
peak:144	138841628	138842123	495	138780040	138852331	ECSCR	138841628	138842123

peak:145	149531548	149532482	934	149504776	149540883	PDGFRB	149531548	149532482
peak:146	153628730	153629524	794	153494408	153751441	GALNT10	153628730	153629524
peak:147	168710264	168710743	479	168709416	168869385	SLIT3	168710264	168710743
peak:148	168720216	168724104	3888	168709416	168869385	SLIT3	168720216	168724104
peak:149	171607930	171608476	546	171524612	171618261	STK10	171607930	171608476
peak:150	173321859	173322378	519	173179499	173386363	CPEB4	173321859	173322378
peak:151	178013980	178014644	664	177678584	178035805	COL23A1	178013980	178014644
peak:152	179767625	179769376	1751	179749694	179850866	GFPT2	179767625	179769376
peak:153	24904932	24905894	962	24826613	25090224	FAM65B	24904932	24905894
peak:154	33789984	33790510	526	33764350	33816160	MLN	33789984	33790510
peak:155	41906137	41906900	763	41899055	42017430	CCND3	41906137	41906900
peak:156	43069195	43070889	1694	43036095	43119539	PTK7	43069195	43070889
peak:157	44670589	44671034	445	44379315	44738564	MIR4642	44670589	44671034
peak:158	44671581	44672269	688	44379315	44738564	MIR4642	44671581	44672269
peak:159	86163397	86164057	660	85816629	86218751	NT5E	86163397	86164057
peak:160	91226084	91226619	535	91134700	91764199	MAP3K7	91226084	91226619
peak:161	98343495	98344020	525	98167346	98877493	MIR2113	98343495	98344020
peak:162	138809524	138810570	1046	138788506	138953236	NHSL1	138809524	138810570
peak:163	147531349	147531922	573	147526429	147737961	STXBP5	147531349	147531922
peak:164	157262218	157262772	554	157178733	157500926	ARID1B	157262218	157262772
peak:165	6052643	6053433	790	6048810	6059944	AIMP2	6052643	6053433
peak:166	22258202	22258490	288	22093851	22468217	RAPGEF5	22258202	22258490
peak:167	26074531	26075475	944	25935119	26090726	MIR148A	26074531	26075475
peak:168	27202934	27209614	6680	27200723	27207165	HOXA9	27202934	27207165
peak:168	27202934	27209614	6680	27207166	27211568	MIR196B	27207166	27209614
peak:169	27210826	27219500	8674	27207166	27211568	MIR196B	27210826	27211568
peak:169	27210826	27219500	8674	27211569	27222357	HOXA10	27211569	27219500
peak:170	27232641	27233483	842	27232284	27239882	HOXA13	27232641	27233483
peak:171	27234692	27235912	1220	27232284	27239882	HOXA13	27234692	27235912
peak:172	27281139	27284013	2874	27261103	27485780	EVX1	27281139	27284013
peak:173	27811436	27811765	329	27740807	27905694	TAX1BP1	27811436	27811765
peak:174	29700851	29701893	1042	29661936	29722607	MIR550A3	29700851	29701893
peak:175	29702454	29703401	947	29661936	29722607	MIR550A3	29702454	29703401
peak:176	29716072	29717020	948	29661936	29722607	MIR550A3	29716072	29717020
peak:177	29717084	29718133	1049	29661936	29722607	MIR550A3	29717084	29718133
peak:178	30960869	30961483	614	30924392	30982377	AQP1	30960869	30961483
peak:179	32328879	32329394	515	31918549	32434203	PDE1C	32328879	32329394
peak:180	33958414	33958857	443	33667270	34321210	BMPER	33958414	33958857
peak:181	35284954	35285617	663	35259743	35514228	TBX20	35284954	35285617
peak:182	43695681	43696256	575	43406594	43695916	STK17A	43695681	43695916
peak:182	43695681	43696256	575	43695917	43783706	COA1	43695917	43696256
peak:183	79765871	79770957	5086	79582357	79881981	GNAI1	79765871	79770957
peak:184	94029143	94029692	549	93828782	94093103	COL1A2	94029143	94029692
peak:185	97950456	97951212	756	97896272	97970703	BRI3	97950456	97951212
peak:186	1780828	1781459	631	1768774	1876422	ARHGEF10	1780828	1781459
peak:187	10582724	10583330	606	10559085	10635487	SOX7	10582724	10583330
peak:188	20038777	20039619	842	19918650	20047710	SLC18A1	20038777	20039619
peak:189	37669114	37669986	872	37637252	37680916	ADGRA2	37669114	37669986
peak:190	37670156	37670966	810	37637252	37680916	ADGRA2	37670156	37670966
peak:191	37897298	37898459	1161	37856103	37925515	EIF4EBP1	37897298	37898459

peak:192	48864485	48865178	693	48761735	48872753	PRKDC	48864485	48865178
peak:193	49295108	49296034	926	49284433	49740934	EFCAB1	49295108	49296034
peak:194	49828980	49834100	5120	49740935	49900447	SNAI2	49828980	49834100
peak:195	58969532	58970281	749	58549608	59115468	FAM110B	58969532	58970281
peak:196	79428973	79429516	543	78670809	79540874	PKIA	79428973	79429516
peak:197	93033549	93034137	588	92632817	93456871	RUNX1T1	93033549	93034137
peak:198	95445551	95448329	2778	95361864	95513467	RAD54B	95445551	95448329
peak:199	102524986	102525522	536	102442895	102654053	GRHL2	102524986	102525522
peak:200	102546839	102547518	679	102442895	102654053	GRHL2	102546839	102547518
peak:201	106337054	106338228	1174	105966200	106992762	ZFPM2	106337054	106338228
peak:202	106338309	106340334	2025	105966200	106992762	ZFPM2	106338309	106340334
peak:203	106340804	106341562	758	105966200	106992762	ZFPM2	106340804	106341562
peak:204	106374855	106375487	632	105966200	106992762	ZFPM2	106374855	106375487
peak:205	106380509	106381181	672	105966200	106992762	ZFPM2	106380509	106381181
peak:206	106381391	106382004	613	105966200	106992762	ZFPM2	106381391	106382004
peak:207	106413579	106414280	701	105966200	106992762	ZFPM2	106413579	106414280
peak:208	124169312	124169710	398	124164792	124211184	FAM83A	124169312	124169710
peak:209	144771302	144772218	916	144749289	144772953	ZNF707	144771302	144772218
peak:210	16484326	16485027	701	16356917	17002912	BNC2	16484326	16485027
peak:211	16789404	16790188	784	16356917	17002912	BNC2	16789404	16790188
peak:212	16828950	16832075	3125	16356917	17002912	BNC2	16828950	16832075
peak:213	16832166	16832985	819	16356917	17002912	BNC2	16832166	16832985
peak:214	16833064	16835139	2075	16356917	17002912	BNC2	16833064	16835139
peak:215	16835678	16838916	3238	16356917	17002912	BNC2	16835678	16838916
peak:216	16841587	16845686	4099	16356917	17002912	BNC2	16841587	16845686
peak:217	16850699	16852788	2089	16356917	17002912	BNC2	16850699	16852788
peak:218	16853303	16855571	2268	16356917	17002912	BNC2	16853303	16855571
peak:219	16855770	16857548	1778	16356917	17002912	BNC2	16855770	16857548
peak:220	16864908	16866306	1398	16356917	17002912	BNC2	16864908	16866306
peak:221	18549881	18550727	846	18523692	18699720	MIR3152	18549881	18550727
peak:222	20693805	20694368	563	20687207	20768198	MIR491	20693805	20694368
peak:223	27126520	27127273	753	27057420	27220305	TEK	27126520	27127273
peak:224	27142964	27143524	560	27057420	27220305	TEK	27142964	27143524
peak:225	34116427	34117310	883	34087860	34152887	DCAF12	34116427	34117310
peak:226	37992368	37992931	563	37986781	38230935	SHB	37992368	37992931
peak:227	108027552	108028747	1195	107848729	108164036	SLC44A1	108027552	108028747
peak:228	108031856	108032804	948	107848729	108164036	SLC44A1	108031856	108032804
peak:229	111650827	111651505	678	111639663	111696640	IKBKAP	111650827	111651505
peak:230	112547947	112548821	874	112331831	112676727	PALM2	112547947	112548821
peak:231	124128773	124129673	900	124103166	124197444	STOM	124128773	124129673
peak:232	125796359	125797211	852	125749611	125836839	GPR21	125796359	125797211
peak:233	125800184	125800852	668	125749611	125836839	GPR21	125800184	125800852
peak:234	126129800	126131502	1702	126074652	126141665	CRB2	126129800	126131502
peak:235	130317788	130318293	505	130294416	130357877	FAM129B	130317788	130318293
peak:236	134147587	134148770	1183	134106696	134158493	FAM78A	134147587	134148770
peak:237	134149070	134152060	2990	134106696	134158493	FAM78A	134149070	134152060
peak:238	137616525	137617372	847	137421328	137637433	COL5A1	137616525	137617372
peak:239	138973618	138974226	608	138920179	138998704	NACC2	138973618	138974226
peak:240	139423069	139424634	1565	139411041	139427158	MIR4673	139423069	139424634
peak:241	1093416	1094782	1366	1081438	1095269	IDI1	1093416	1094782

peak:242	6144391	6145180	789	6117642	6171484	RBM17	6144391	6145180
peak:243	24633820	24634513	693	24554436	24651604	MIR603	24633820	24634513
peak:244	29946523	29947035	512	29907589	30187176	SVIL	29946523	29947035
peak:245	30329105	30330584	1479	30187177	30521343	KIAA1462	30329105	30330584
peak:246	33602986	33604361	1375	33435531	33842807	NRP1	33602986	33604361
peak:247	33612310	33623591	11281	33435531	33842807	NRP1	33612310	33623591
peak:248	69524126	69524508	382	69055605	69526943	CTNNA3	69524126	69524508
peak:249	71563416	71564435	1019	71475824	71687000	COL13A1	71563416	71564435
peak:250	72972242	72977264	5022	72810417	73025651	UNC5B	72972242	72977264
peak:251	80947229	80947935	706	80828665	81086538	ZMIZ1	80947229	80947935
peak:252	88716692	88717151	459	88616911	88717856	MMRN2	88716692	88717151
peak:253	91155250	91155882	632	91145059	91163314	IFIT1	91155250	91155882
peak:254	104552485	104553797	1312	104489013	104566589	WBP1L	104552485	104553797
peak:255	104559723	104560312	589	104489013	104566589	WBP1L	104559723	104560312
peak:256	112837909	112838721	812	112780337	113390129	ADRA2A	112837909	112838721
peak:257	116158426	116160362	1936	116034844	116208076	AFAP1L2	116158426	116160362
peak:258	123244575	123245599	1024	122927677	123522759	FGFR2	123244575	123245599
peak:259	130381649	130382040	391	129885908	130594961	MKI67	130381649	130382040
peak:260	2017705	2019003	1298	1993282	2018563	MIR675	2017705	2018563
peak:260	2017705	2019003	1298	2018564	2087252	H19	2018564	2019003
peak:261	2160943	2164498	3555	2156971	2176525	IGF2	2160943	2164498
peak:262	11268043	11268592	549	11127263	11509232	CSNK2A3	11268043	11268592
peak:263	12402647	12403252	605	12353737	12557878	PARVA	12402647	12403252
peak:264	12404587	12407120	2533	12353737	12557878	PARVA	12404587	12407120
peak:265	12410514	12411161	647	12353737	12557878	PARVA	12410514	12411161
peak:266	12414622	12416345	1723	12353737	12557878	PARVA	12414622	12416345
peak:267	12834669	12835287	618	12557879	12956175	TEAD1	12834669	12835287
peak:268	16566539	16567254	715	15797531	16694225	SOX6	16566539	16567254
peak:269	16592793	16593551	758	15797531	16694225	SOX6	16592793	16593551
peak:270	16609429	16610177	748	15797531	16694225	SOX6	16609429	16610177
peak:271	16615703	16616149	446	15797531	16694225	SOX6	16615703	16616149
peak:272	16623340	16624503	1163	15797531	16694225	SOX6	16623340	16624503
peak:273	27433611	27434180	569	27230870	27439564	CCDC34	27433611	27434180
peak:274	44798075	44798691	616	44686559	44949858	TSPAN18	44798075	44798691
peak:275	46377734	46378238	504	46345834	46390548	DGKZ	46377734	46378238
peak:276	48050352	48050895	543	47936084	48197802	PTPRJ	48050352	48050895
peak:277	61534047	61535299	1252	61523999	61535107	DKFZP434K(	61534047	61535107
peak:277	61534047	61535299	1252	61535108	61552555	MYRF	61535108	61535299
peak:278	66486509	66487328	819	66450413	66500538	SPTBN2	66486509	66487328
peak:279	66493674	66495379	1705	66450413	66500538	SPTBN2	66493674	66495379
peak:280	82581850	82582560	710	82528232	82612147	PRCP	82581850	82582560
peak:281	82583067	82583651	584	82528232	82612147	PRCP	82583067	82583651
peak:282	85194858	85195323	465	83195442	85338965	DLG2	85194858	85195323
peak:283	114316541	114317397	856	114290747	114355869	REXO2	114316541	114317397
peak:284	121332485	121333650	1165	121243245	121715840	SORL1	121332485	121333650
peak:285	128361238	128362192	954	127632781	128506941	ETS1	128361238	128362192
peak:286	128600867	128601738	871	128596965	128670219	FLI1	128600867	128601738
peak:287	129984417	129985076	659	129906224	130019573	APLP2	129984417	129985076
peak:288	133953655	133955119	1464	133882735	134016623	JAM3	133953655	133955119
peak:289	133956162	133956636	474	133882735	134016623	JAM3	133956162	133956636

peak:290	11830639	11831672	1033	11751877	12123118	ETV6	11830639	11831672
peak:291	20704229	20704633	404	20057848	20786543	PDE3A	20704229	20704633
peak:292	33592073	33592479	406	33321268	33883985	SYT10	33592073	33592479
peak:293	34372437	34372829	392	33883986	36442886	ALG10	34372437	34372829
peak:294	47468861	47473585	4724	47346584	47473560	PCED1B	47468861	47473560
peak:294	47468861	47473585	4724	47473561	47527664	AMIGO2	47473561	47473585
peak:295	48578048	48580774	2726	48564372	48587220	CCDC184	48578048	48580774
peak:296	48581132	48581632	500	48564372	48587220	CCDC184	48581132	48581632
peak:297	48740759	48744225	3466	48733719	48805738	ZNF641	48740759	48744225
peak:298	50095140	50096362	1222	50035177	50118245	FMNL3	50095140	50096362
peak:299	51319023	51320625	1602	51277618	51333292	METTL7A	51319023	51320625
peak:300	54411997	54412633	636	54406767	54424513	HOXC6	54411997	54412633
peak:301	54422385	54422911	526	54406767	54424513	HOXC6	54422385	54422911
peak:302	54520010	54522014	2004	54517390	54604019	SMUG1	54520010	54522014
peak:303	54526117	54526871	754	54517390	54604019	SMUG1	54526117	54526871
peak:304	62661805	62662398	593	62654024	62757359	USP15	62661805	62662398
peak:305	76945776	76946352	576	76779548	77055721	OSBPL8	76945776	76946352
peak:306	91497059	91498160	1101	91478837	91538952	LUM	91497059	91498160
peak:307	91566883	91567833	950	91538953	92056147	DCN	91566883	91567833
peak:308	91572618	91573569	951	91538953	92056147	DCN	91572618	91573569
peak:309	95535046	95536009	963	95499430	95611381	FGD6	95535046	95536009
peak:310	95539092	95539807	715	95499430	95611381	FGD6	95539092	95539807
peak:311	96423196	96423846	650	96399548	96512752	LTA4H	96423196	96423846
peak:312	96601230	96602388	1158	96512753	96691286	ELK3	96601230	96602388
peak:313	109227249	109229598	2349	109162144	109252033	SSH1	109227249	109229598
peak:314	111855696	111856834	1138	111825339	111890655	SH2B3	111855696	111856834
peak:315	111860717	111861162	445	111825339	111890655	SH2B3	111860717	111861162
peak:316	116460997	116461510	513	115854215	116650725	MIR620	116460997	116461510
peak:317	116462513	116463600	1087	115854215	116650725	MIR620	116462513	116463600
peak:318	116465234	116466269	1035	115854215	116650725	MIR620	116465234	116466269
peak:319	116466391	116469400	3009	115854215	116650725	MIR620	116466391	116469400
peak:320	116476688	116479586	2898	115854215	116650725	MIR620	116476688	116479586
peak:321	29052854	29053736	882	28815491	29151203	FLT1	29052854	29053736
peak:322	70834842	70835388	546	70681986	71135949	KLHL1	70834842	70835388
peak:323	97886176	97888570	2394	97720348	98042885	MBNL2	97886176	97888570
peak:324	97888978	97890385	1407	97720348	98042885	MBNL2	97888978	97890385
peak:325	113424650	113425196	546	113323001	113559702	ATP11A	113424650	113425196
peak:326	114844483	114845177	694	114716817	114949228	RASA3	114844483	114845177
peak:327	114862352	114862769	417	114716817	114949228	RASA3	114862352	114862769
peak:328	114874693	114876466	1773	114716817	114949228	RASA3	114874693	114876466
peak:329	114878447	114879160	713	114716817	114949228	RASA3	114878447	114879160
peak:330	27858359	27859154	795	27729822	28659036	LINC00645	27858359	27859154
peak:331	52513146	52521420	8274	52496088	52635188	NID2	52513146	52521420
peak:332	64966283	64967079	796	64951386	64970628	ZBTB25	64966283	64967079
peak:333	65194298	65196221	1923	65112010	65227024	PLEKHG3	65194298	65196221
peak:334	75745948	75747572	1624	75694416	75753726	FOS	75745948	75747572
peak:335	75911206	75912346	1140	75827809	75943810	JDP2	75911206	75912346
peak:336	41225335	41225921	586	41204080	41233583	DLL4	41225335	41225921
peak:337	50400402	50401262	860	50040977	50442906	ATP8B4	50400402	50401262
peak:338	53827799	53828339	540	53457630	54180088	WDR72	53827799	53828339

peak:339	55255684	55256393	709	55195386	55525856	RSL24D1	55255684	55256393
peak:340	57680561	57685031	4470	57630634	57776402	CGNL1	57680561	57685031
peak:341	60661001	60661414	413	60493304	60718084	ANXA2	60661001	60661414
peak:342	68132224	68132783	559	68022467	68229307	SKOR1	68132224	68132783
peak:343	78361246	78361773	527	78149052	78372934	TBC1D2B	78361246	78361773
peak:344	83939486	83940588	1102	83914419	84034779	BNC1	83939486	83940588
peak:345	23137116	23137663	547	22954865	23177315	USP31	23137116	23137663
peak:346	33962904	33963356	452	33612312	34183632	LINC00273	33962904	33963356
peak:347	65122252	65122769	517	63554842	65276815	CDH11	65122252	65122769
peak:348	65275625	65276174	549	63554842	65276815	CDH11	65275625	65276174
peak:349	65280051	65280935	884	65276816	66005364	LINC00922	65280051	65280935
peak:350	67499011	67499644	633	67479083	67516402	ATP6V0D1	67499011	67499644
peak:351	68706305	68706780	475	68625907	68724673	CDH3	68706305	68706780
peak:352	75489293	75490494	1201	75482851	75513755	TMEM170A	75489293	75490494
peak:353	77465736	77467040	1304	77321978	77612700	ADAMTS18	77465736	77467040
peak:354	84865362	84867141	1779	84793572	84949364	CRISPLD2	84865362	84867141
peak:355	84867188	84868387	1199	84793572	84949364	CRISPLD2	84867188	84868387
peak:356	86537415	86539157	1742	86460876	86543299	FENDRR	86537415	86539157
peak:357	86539384	86541739	2355	86460876	86543299	FENDRR	86539384	86541739
peak:358	86544002	86551528	7526	86543300	86566243	FOXF1	86544002	86551528
peak:359	4411509	4412371	862	4369675	4442887	SPNS2	4411509	4412371
peak:360	4412486	4413888	1402	4369675	4442887	SPNS2	4412486	4413888
peak:361	7611015	7611676	661	7606290	7614799	EFNB3	7611015	7611676
peak:362	15146073	15146631	558	15044653	15159553	MIR4731	15146073	15146631
peak:363	15152152	15152660	508	15044653	15159553	MIR4731	15152152	15152660
peak:364	15154738	15155824	1086	15044653	15159553	MIR4731	15154738	15155824
peak:365	15156973	15157873	900	15044653	15159553	MIR4731	15156973	15157873
peak:366	15161580	15163773	2193	15159554	15206801	PMP22	15161580	15163773
peak:367	20783982	20784869	887	20641246	20872902	CCDC144NL	20783982	20784869
peak:368	25850578	25851670	1092	25772034	25947557	KSR1	25850578	25851670
peak:369	28457021	28457549	528	28444138	28463722	MIR3184	28457021	28457549
peak:370	29907826	29908340	514	29902360	30044378	MIR365B	29907826	29908340
peak:371	36610107	36610693	586	36546364	36669058	ARHGAP23	36610107	36610693
peak:372	36613351	36614272	921	36546364	36669058	ARHGAP23	36613351	36614272
peak:373	40513617	40514505	888	40499324	40557893	STAT3	40513617	40514505
peak:374	46641880	46654040	12160	46626315	46654090	HOXB3	46641880	46654040
peak:375	46655944	46662212	6268	46654091	46656526	HOXB4	46655944	46656526
peak:375	46655944	46662212	6268	46656527	46658562	MIR10A	46656527	46658562
peak:375	46655944	46662212	6268	46658563	46669367	HOXB3	46658563	46662212
peak:376	46662319	46671164	8845	46658563	46669367	HOXB3	46662319	46669367
peak:376	46662319	46671164	8845	46669368	46676718	HOXB5	46669368	46671164
peak:377	46671218	46685602	14384	46669368	46676718	HOXB5	46671218	46676718
peak:377	46671218	46685602	14384	46676719	46685368	HOXB6	46676719	46685368
peak:377	46671218	46685602	14384	46685369	46690342	HOXB7	46685369	46685602
peak:378	46698382	46701475	3093	46698069	46706878	HOXB9	46698382	46701475
peak:379	46701835	46703183	1348	46698069	46706878	HOXB9	46701835	46703183
peak:380	48134857	48135604	747	48102965	48152720	ITGA3	48134857	48135604
peak:381	60727017	60728343	1326	60631619	60821415	MRC2	60727017	60728343
peak:382	62610344	62610838	494	62593672	62738303	SMURF2	62610344	62610838
peak:383	72425330	72425990	660	72395657	72450873	GPRC5C	72425330	72425990

peak:384	73677273	73677974	701	73663335	73690457	SAP30BP	73677273	73677974
peak:385	78526234	78527056	822	78484515	78944438	RPTOR	78526234	78527056
peak:386	81042045	81046708	4663	81023627	81108307	METRNL	81042045	81046708
peak:387	6730641	6740773	10132	6649955	6889670	ARHGAP28	6730641	6740773
peak:388	6773975	6775515	1540	6649955	6889670	ARHGAP28	6773975	6775515
peak:389	43771278	43772276	998	43719144	43830380	C18orf25	43771278	43772276
peak:390	53058240	53058853	613	52798296	53138910	TCF4	53058240	53058853
peak:391	11207061	11208924	1863	11165648	11252584	LDLR	11207061	11208924
peak:392	17483803	17484462	659	17468232	17502260	PLVAP	17483803	17484462
peak:393	17486542	17487410	868	17468232	17502260	PLVAP	17486542	17487410
peak:394	24183657	24183873	216	24156966	24308112	ZNF254	24183657	24183873
peak:395	31775147	31775723	576	31740487	31959642	TSHZ3	31775147	31775723
peak:396	31808196	31809598	1402	31740487	31959642	TSHZ3	31808196	31809598
peak:397	31841439	31843763	2324	31740487	31959642	TSHZ3	31841439	31843763
peak:398	31845066	31845687	621	31740487	31959642	TSHZ3	31845066	31845687
peak:399	36066328	36066921	593	36042626	36079103	ATP4A	36066328	36066921
peak:400	54376620	54378204	1584	54348635	54379124	MYADM	54376620	54378204
peak:401	55542916	55543440	524	55513672	55557464	GP6	55542916	55543440
peak:402	587634	588435	801	557697	612462	TCF15	587634	588435
peak:403	17614207	17615256	1049	17588903	17668624	RRBP1	17614207	17615256
peak:404	19969145	19969984	839	19956839	20015798	NAA20	19969145	19969984
peak:405	23026698	23028411	1713	23023180	23048639	THBD	23026698	23028411
peak:406	48599528	48604817	5289	48576214	48628839	SNAI1	48599528	48604817
peak:407	49275133	49275912	779	49227875	49327998	FAM65C	49275133	49275912
peak:408	49304551	49305860	1309	49227875	49327998	FAM65C	49304551	49305860
peak:409	50155602	50155980	378	50114387	50246706	NFATC2	50155602	50155980
peak:410	57464269	57466116	1847	57404082	57517149	GNAS	57464269	57466116
peak:411	9826877	9827690	813	9826018	9897398	MIR3687-1	9826877	9827690
peak:412	15910563	15911212	649	15837096	16196424	SAMSN1	15910563	15911212
peak:413	28211847	28217731	5884	28081655	28272004	ADAMTS1	28211847	28217731
peak:414	29466657	29467408	751	29240191	29648661	LINC00314	29466657	29467408
peak:415	33739292	33739898	606	33718237	33775032	URB1	33739292	33739898
peak:416	38626544	38627209	665	38610319	38689846	DSCR3	38626544	38627209
peak:417	39868629	39869645	1016	39709987	40078942	ERG	39868629	39869645
peak:418	44400848	44402672	1824	44354011	44456475	PKNOX1	44400848	44402672
peak:419	46203226	46203991	765	46176624	46229897	UBE2G2	46203226	46203991
peak:420	46700079	46700967	888	46634925	46766454	POFUT2	46700079	46700967
peak:421	47401672	47407366	5694	47358893	47469572	COL6A1	47401672	47407366
peak:422	47516950	47517447	497	47469573	47540344	COL6A2	47516950	47517447
peak:423	47518597	47531485	12888	47469573	47540344	COL6A2	47518597	47531485
peak:424	47531878	47535394	3516	47469573	47540344	COL6A2	47531878	47535394
peak:425	20788478	20789449	971	20770276	20821158	SCARF2	20788478	20789449
peak:426	26952565	26953742	1177	26929864	26956329	MIR548J	26952565	26953742
peak:427	26975135	26975847	712	26956330	27000040	TPST2	26975135	26975847
peak:428	31647411	31648425	1014	31582195	31665530	LIMK2	31647411	31648425
peak:429	31650134	31650700	566	31582195	31665530	LIMK2	31650134	31650700
peak:430	39873686	39874512	826	39824543	39889667	MGAT3	39873686	39874512
peak:431	41208671	41209275	604	41142620	41212677	MIR4766	41208671	41209275
peak:432	50952415	50953010	595	50946391	50955339	NCAPH2	50952415	50953010
peak:433	45656406	45657062	656	45606113	45956577	MIR222	45656406	45657062

peak:434	64927214	64928223	1009	64829907	65068474	MSN	64927214	64928223
peak:435	131169422	131170423	1001	131060959	131192913	STK26	131169422	131170423

.

peak_overlap
595
941
1943
1022
1047
677
1045
613
830
604
759
1360
688
607
978
1047
2428
1694
620
535
1253
615
815
1902
1072
1020
1342
523
1868
963
645
593
707
634
569
735
793
513
447
542
848
542
2241
1512
1133
595
1118

846
861
454
825
566
1471
704
619
1675
2015
1894
72
4966
1784
1260
3373
396
843
2307
488
774
519
480
3103
538
725
1034
573
702
906
607
1245
602
931
548
1604
781
837
1089
635
1336
1645
664
2031
820
1790
352
604
623
770

504
1253
1122
824
742
573
645
741
592
574
739
1380
787
624
853
846
1528
633
4093
378
467
713
750
504
435
1285
1333
1275
516
706
622
4104
581
851
348
1312
491
981
2391
2035
805
1896
635
580
618
6379
592
681
589
496

935
795
480
3889
547
520
665
1752
963
527
764
1695
446
689
661
536
526
1047
574
555
791
289
945
4232
2449
743
7932
843
1221
2875
330
1043
948
949
1050
615
516
444
664
236
340
5087
550
757
632
607
843
873
811
1162

694
927
5121
750
544
589
2779
537
680
1175
2026
759
633
673
614
702
399
917
702
785
3126
820
2076
3239
4100
2090
2269
1779
1399
847
564
754
561
884
564
1196
949
679
875
901
853
669
1703
506
1184
2991
848
609
1566
1367

790
694
513
1480
1376
11282
383
1020
5023
707
460
633
1313
590
813
1937
1025
392
859
440
3556
550
606
2534
648
1724
619
716
759
749
447
1164
570
617
505
544
1061
192
820
1706
711
585
466
857
1166
955
872
660
1465
475

1034
405
407
393
4700
25
2727
501
3467
1223
1603
637
527
2005
755
594
577
1102
951
952
964
716
651
1159
2350
1139
446
514
1088
1036
3010
2899
883
547
2395
1408
547
695
418
1774
714
796
8275
797
1924
1625
1141
587
861
541

710
4471
414
560
528
1103
548
453
518
550
885
634
476
1202
1305
1780
1200
1743
2356
7527
863
1403
662
559
509
1087
901
2194
888
1093
529
515
587
922
889
12161
583
2036
3650
7049
1797
5501
8650
234
3094
1349
748
1327
495
661

702
823
4664
10133
1541
999
614
1864
660
869
217
577
1403
2325
622
594
1585
525
802
1050
840
1714
5290
780
1310
379
1848
814
650
5885
752
607
666
1017
1825
766
889
5695
498
12889
3517
972
1178
713
1015
567
827
605
596
657

1010
1002